A MODIFIED PULSE SHAPER USING MICROLENS ARRAYS

A Thesis

Submitted to the Faculty

of

Purdue University

by

Keith M. Mahoney

In Partial Fulfillment of the

Requirements for the Degree

of

Master of Science in Electrical Engineering

December 1994

To my wife, parents, teachers, and all those who have instilled in me the desire to learn.

ACKNOWLEDGMENTS

I'd like to thank Shanan for her support and encouragement. I would like to thank Professor Andrew Weiner for the opportunity to work and learn from him and for funding me while working on my Masters.

I would like to thank Corning, NSG America and United Technologies for use of the microlens arrays used in these experiments.

TABLE OF CONTENTS

Page

LIST OF FIGURES

Figure Page

ABSTRACT

Mahoney, Keith M. M.S.E.E., Purdue University, December 1994. A Modified Pulse Shaper Using Microlens Arrays. Major Professor: Weiner, Andrew M.

Shaped femtosecond pulses have been generated by spatial filtering in a zero-dispersion pulse compressor by using fixed pulse shaping masks as well as linear liquid crystal modulator (LCM) arrays that allow pulse shape programmability. In the case of liquid crystal modulators, the gaps between the modulator pixels limit the ability to control some of the optical frequency components. A modified pulse shaper design is described that incorporates microlens arrays to avoid interpixel gaps, and preliminary experimental results are presented. The modified pulse shaper is potentially applicable not only to linear liquid crystal arrays, but also to 2-D liquid crystal arrays, SEEDs and other pixellated devices.

The goal is to utilize microlens arrays to convert the continuous band of frequency components normally found in the Fourier plane of a pulse shaper into a series of discrete spots which could correspond to the center-to-center spacing of a pixellated modulator. The system was designed by performing a computer ray-tracing analysis using 4 by 4 ray-pulse matrices for dispersive optical systems. With the proper positioning of the microlens arrays in the pulse shaper, the pulse should emerge from the shaper as a collimated beam without dispersive broadening. Initial experiments (without a mask or modulator array) have been performed to test the dispersive properties of the modified pulse shaper. The deconvolved pulse duration of the output pulses from the modified pulse shaper is close to the width of the output pulse without the microlens arrays. This demonstrates that no appreciable dispersion is added to the input pulse by the addition of the microlens arrays to the pulse shaper. I am continuing this research by fabricating a series of fixed amplitude masks with gaps of

various dimensions purposely included. Insertion of these masks into the pulse shaper should provide experimental data testing how well the microlens arrays improve the pulse shaping performance of pixellated masks.

1. INTRODUCTION

A zero-dispersion pulse compressor has been used for many years as a way to shape femtosecond pulses [1]. This is done by spatially filtering the frequency components of a pulse. This can be done with fixed lithographic masks or liquid crystal modulators. Liquid crystal modulators have been used to generate femtosecond pulse shaping with electronic programmability [2]. Initially, this was done with a linear array of 32 pixels that were spaced at 100 μm center and had 5 μm gaps. Work has been done to increase the number of pixels and decrease the size of the gaps. A 128-element liquid crystal modulator with 40 μm center-to-center spacing and 2.5 μm gaps was specially fabricated for use inside a pulse shaper [3]. Now, commercially made liquid crystal modulators are being fabricated that have 128 pixels that have 100 μm center-to-center spacing and 3 μm gaps. The manufacturing process needed to produce modulators with 3 μm gaps is very demanding. Insuring that all of the pixels are active and that there are no shorts between neighboring pixels is a difficult task. For modulators that have 5 μm gaps, manufacturing techniques are able to consistently produce quality liquid crystal pixellated arrays. The interpixel gaps cause the liquid crystal modulators to have lower resolution than the fixed masks. The interpixel gaps cause satellite pulses to occur before and after the shaped pulse. These satellite pulses could be undesirable to the optical system that uses the shaped pulses. Microlens arrays could be used to reduce the satellite pulses caused by the interpixel gaps and provide better resolution.

A colliding-pulse-mode-locked (CPM) dye laser, described in detail in a later section, is used to generate femtosecond pulses used in these experiments. Microlens are being produced that have diameters on the order of hundreds of micrometers [4] [5].

These microlens can be binary optic lenses [6] or distributed index lenses [7]. The imaging properties of these microlens have been analyzed [8] [9] [10] [11] for use with LCD projector [12], optical fibers [13] , optical interconnects [14], and array generation [15]. One type of distributed index lenses is produced by molding an optical epoxy onto a substrate [4]. This method produces a microlens array that has satisfactory imaging characteristics. I have experimentally tested and calculated the microlens imaging efficiency for that microlens array.

The use of microlens inside a pulse shaper must keep the pulse shaper dispersion-free and produce a collimated output pulse. In order to design a geometry that would adhere to those guidelines, computer calculations were performed with numerous geometries. Ray tracing using 4 by 4 matrices were used to account for the dispersive properties of the optical components used inside the modified pulse shaper [16]. These matrices were tested by analyzing a conventional pulse shaper to compare the computational results with known experimental and theoretical results. The exact position of the microlens arrays was computed and the location of the plane to use for spatial filtering was found. Many possible microlens arrays were analyzed to select the microlens with the best diameter and focal length.

Testing was done on the modified pulse shaper to measure how well the microlens performs inside the pulse shaper without any mask or modulator in place. The pulsewidth was recorded and compared to the output pulse without the microlens in the pulse shaper to prove that the addition of the microlens arrays kept the modified pulse shaper dispersion-free. The output pulse was recorded and analyzed to see if any undesirable features were present. Future experiments will use fixed masks that model the pixels and interpixel gaps present in a modulator. The output pulse shapes generated by the modified pulse with the masks will be compared to the results generated when using the masks in a conventional pulse shaper. The difference between the two results will provide concrete data showing to what extent microlens arrays improve a pulse shaper that uses pixellated modulators.

2. PULSE SHAPER

2.1 Introduction

Pulse shaping has been used to modify femtosecond pulses to modulate information onto the pulses or to give the pulse a characteristic shape [1]. This is done with spatial filtering in a compressor using fixed masks [17] or linear liquid crystal modulators [3]. The pulse shaper is zero-dispersion, which means that all the frequency components travel the exact same distance. This is important for femtosecond pulses because a frequency dependent path length causes the femtosecond pulse to spread out and become broader. The geometry that performs this operation is shown in figure 2.1. The spacing between the grating and the lens and the distance between the lens and the maskplane is the bulk lens focal length, f. The input beam is directed onto the grating on the right. The first grating separates the frequency components of the input pulse and diffracts them onto the lens. The lens collimates the frequency components of the short pulse such that they are all parallel. The second lens and grating perform the inverse operation as the first set and combine the frequency components so that the frequency components combine and produce an output pulse. At the maskplane (which is halfway between the two lens), the spread of frequency components is the exact Fourier transform of the output pulse in the time domain. Any filtering of the frequency components will change the output in the time domain, which can be calculated by taking the Fourier transform of the spatial filter used at the mask plane. If there is no mask placed between the two lenses the output pulse is the same as the input pulse. A fixed amplitude or phase mask [17], liquid crystal modulator [3], acousto-optic modulator [18], or holographic plate [19] can be placed at the maskplane to filter or record the frequencies.

The connection between the spatial dimensions in the maskplane of the pulse shaper and the frequencies of the femtosecond pulse is an important relationship. It is used when calculating the spatial filtering that should be done to produce a specific pulse shape. Pulse shaping can be described as time-domain Fourier optics. This means that the grating and lens map the optical frequency spectrum onto the filter plane. A spatially patterned mask at the filter plane is used to manipulate the Fourier spectrum. The filter plane is a exact Fourier transform of the output pulse in the time domain. The spatial spread of the frequency components at the mask plane are given by $\partial\lambda/\partial x = (d \cos \theta_d)/f$, where f is the focal length of the lens, d is the period of the grating, and θ_d is the diffraction angle [17]. In this experiment, f = 150 mm, $1/d = 1800$ mm^{-1}, and $\theta_d = 35°$, which gives a $\partial\lambda/\partial x = 3.03$ nm/mm. The bandwidth of the CPM is $\sim$ 10 nm FWHM which corresponds to approximately 5 mm to include the entire spectrum.

2.2 Fixed Mask

By using microlithography, a mask can be fabricated on a fused silica optical window so that the amplitude and phase of the individual frequency components are precisely controlled [17]. The amplitude is controlled by evaporating an partially opaque film of metal onto the fused silica. The phase mask is fabricated by reactive-ion etching to vary the thickness of the mask. As the frequencies travel through the mask, they pass through different amounts of glass and pick up a phase shift relative to the neighboring frequencies. The microlithographic mask imparts a desired amplitude and phase shift on the frequency components that make up the pulse and modifies the output pulse shape. The advantage of this technique is that the masks can be made with very high precision (1 micron resolution) and can modulate both the amplitude and binary phase.

2.3 Liquid Crystal Modulator

Liquid crystal modulators have also been placed in the mask plane and used to modulate the amplitude or phase of the various frequencies. Amplitude modulation of the frequencies at the mask plane will attenuate specific frequency components. The Fourier transform of the output filter plane will produce the output pulse shape. Phase modulation is more efficient because the amplitude response is constant [20]. The phase filtering adds a relative delay compared to the neighboring frequencies. Like the amplitude modulator, taking the Fourier transform of the phase modulator will give the output pulse. Since all of the light passes through the phase modulator, unlike the amplitude modulator, there is a higher efficiency with phase modulation. These linear liquid crystal modulators are made up of individual pixels. Figure 2.2 shows a typical liquid crystal modulator. The pixels are independently driven at different voltage levels. When the liquid crystal modulator, is turned off, the temporal shape of the output pulse is the same as the input. The liquid crystal modulator can provide continuous variable gray-level control of each pixel as compared to the fixed control possible with the masks. The liquid crystal modulator can also provide electronically programmable shaping of pulses in millisecond time by computer control. The typical gaps for a liquid crystal modulator are 2.5-15 μm. The size of the gaps is limited by the microlithographic techniques used to produce the linear array. Improvements in microlithography will allow arrays to be produced with smaller and smaller gaps.

2.3.1 Consequence of Interpixel Gaps

The gaps between the modulator pixels decrease the quality of the pulse shapes that can be produced. The optical frequencies that pass through the gaps cannot be controlled by the modulating voltage. This means that the complete spread of frequency spectrum cannot be completely controlled. Figure 2.3 is a example of a fabricated mask that has pixels with varying widths and interpixel gaps. The mask is a 3 mm single slit which will pass 9.09 nm bandwidth of optical frequencies. Assuming

that the spectrum is flat over the whole 9.09 nm range, the mask will produce a output pulse shape that is a sinc function given by

$$E(t) = E_o \frac{\sin(\pi \Delta f t)}{(\pi \Delta f t)},$$

where Δf is the bandwidth. The duration of the sinc-function is 145 femtoseconds FWHM. The 3 mm slit on the bottom is 0% deadspace which corresponds to 100 μm wide pixel with zero interpixel gap. The next higher slit has 90 μm pixels with a gap of 10 μm. The next three slits have pixels widths and interpixel gaps of 80 μm and 20 μm, 70 μm and 30 μm, and 50 μm and 50 μm. Figure 2.4 through 2.8 are plots of pulse intensity versus time for the calculated temporal pulse shapes corresponding to the spatial filtering by the masks in Figure 2.3. The frequencies hitting the gaps were assumed to be completely absorbed and the frequency components hitting the pixels had no attenuation. The calculated output pulse shape was the Fourier transform assuming the above conditions for the pixels and gaps. As seen by the figures, the peak amplitude of the pulse decreases as the interpixel gaps increase. But more importantly, sidelobes start to be generated that correspond to the inverse frequency spread of the pixel to pixel spacing. The disappearance of the sidelobes at $\pm$ 8.6 psec in figure 2.8 is a side effect of the pixels having the same width as the gaps. These sidelobes degrade the quality of the shaped pulses and create satellite pulses that could cause problems when only a single shaped pulse is desired.

2.3.2 Use of Microlens to Avoid Interpixel Gaps

Microlens Arrays exist that are arranged into arrays of $\sim$ 100 μm diameter microlenses. These microlenses can be incorporated into the pulse shaper to avoid the interpixel gaps and potentially improve the quality of the pulse generated by the modulator arrays. The goal of the microlens array is to convert the continuous band of frequency components normally found in the Fourier plane of a pulse shaper into a series of discrete spots which could correspond to the center-to-center spacing of a pixellated modulator

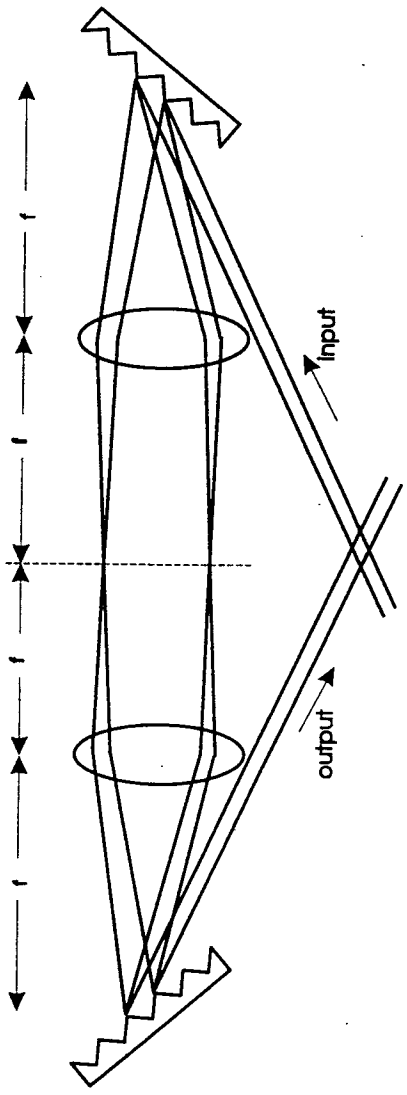

Figure 2.1 Conventional Pulse Shaper

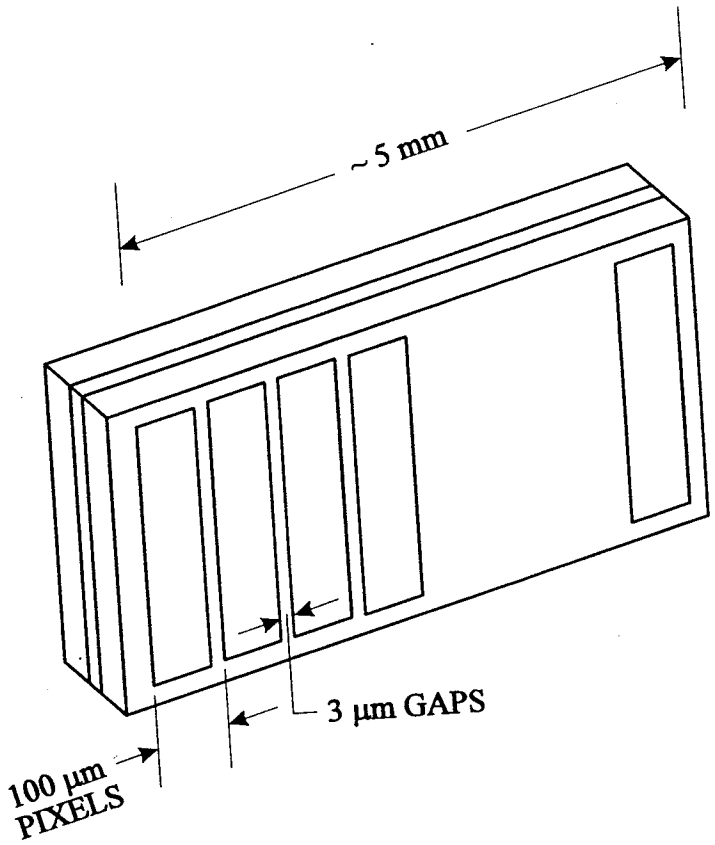

Figure 2.2 Liquid Crystal Modulator

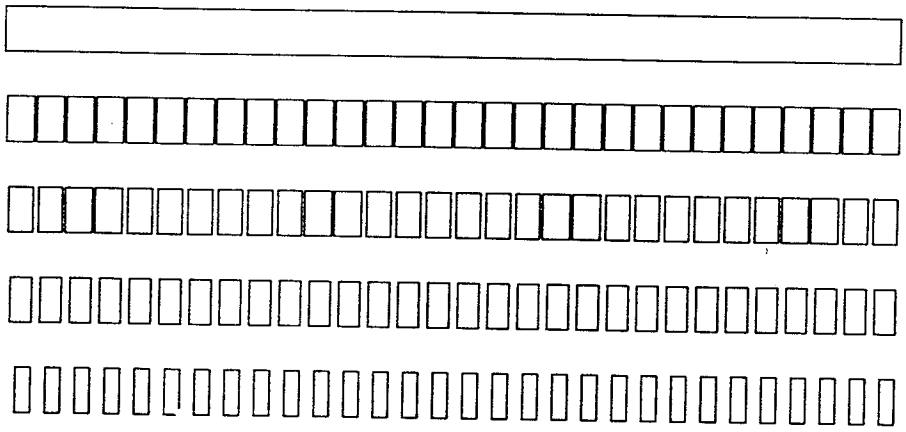

Figure 2.3 Pixellated Modulator Array

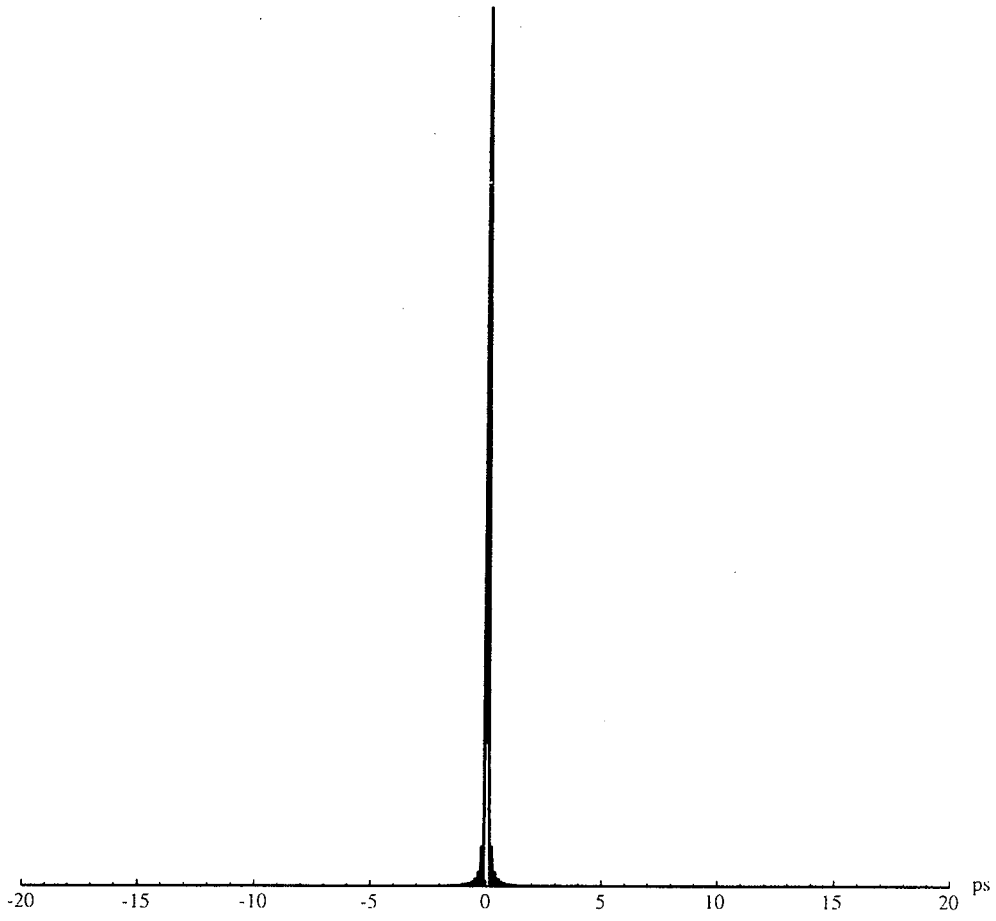

Figure 2.4 Result of 0 % Dead Space

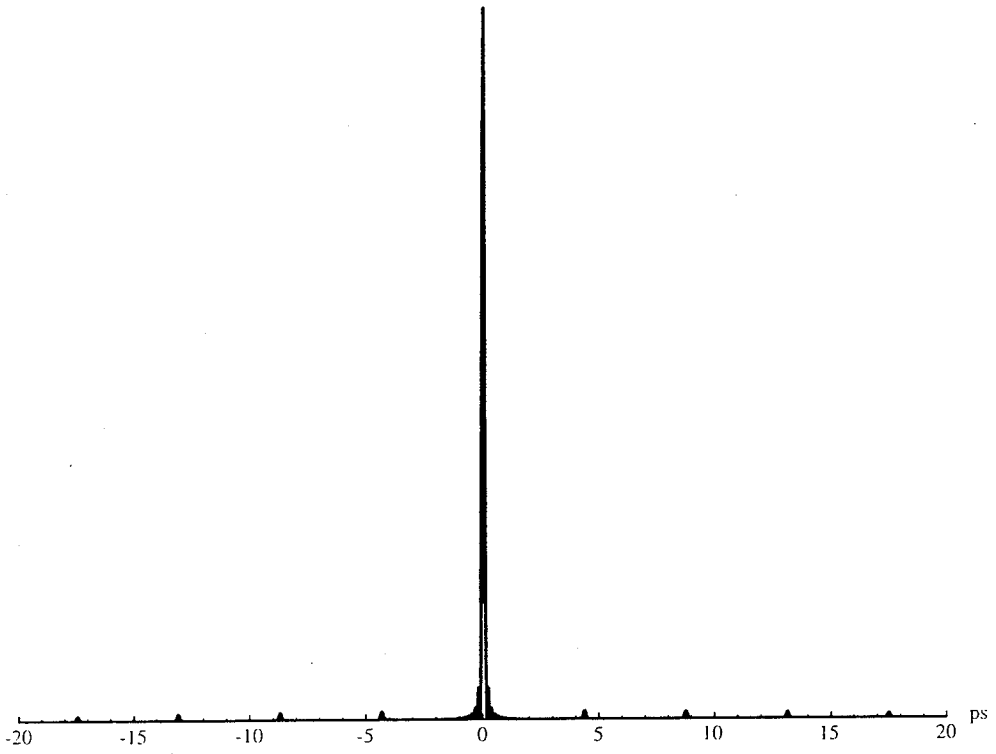

Figure 2.5 Result of 10 % Dead Space

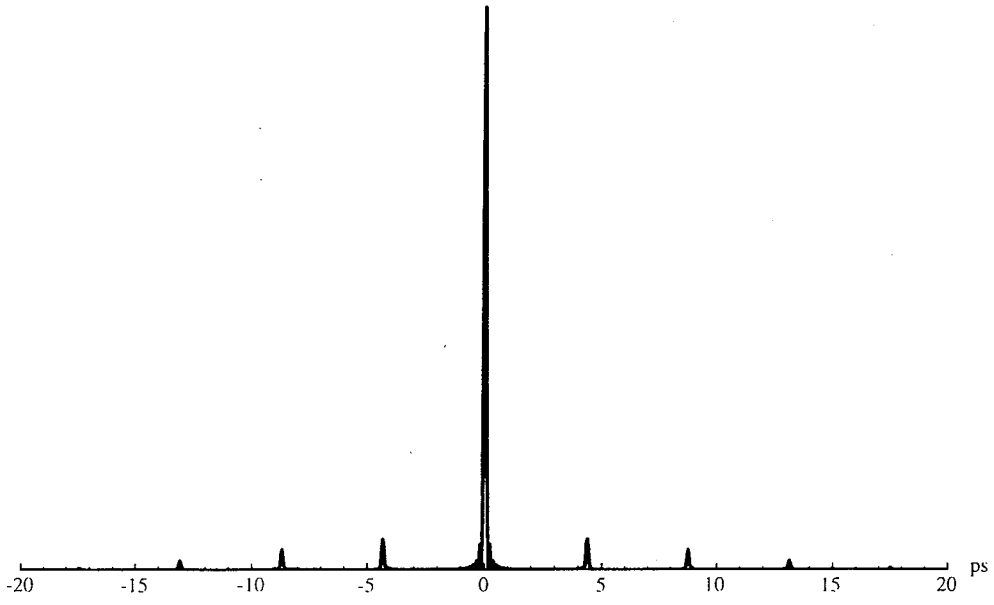

Figure 2.6 Result of 20 % Dead Space

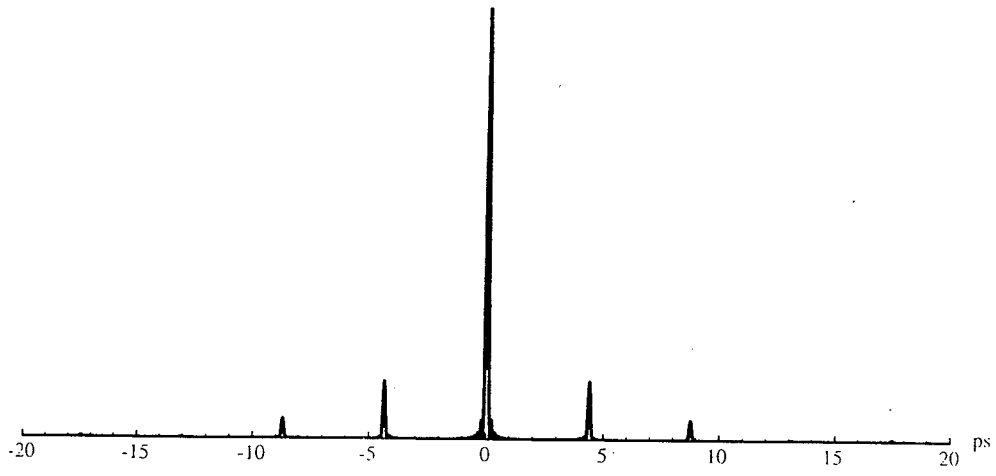

Figure 2.7 Result of 30 % Dead Space

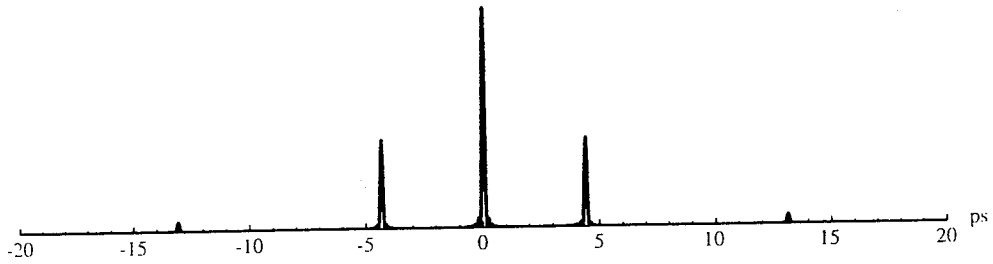

Figure 2.8 Result of 50 % Dead Space

3. ULTRASHORT PULSES

3.1 Generation of Ultrashort Pulses

The shortest femtosecond pulses have been generated using passive mode-locking. The passive mode-locked dye laser used in these experiments is called a colliding-pulse-mode-locked(CPM) ring dye laser [21] [22] and shown in figure 3.1. The CPM laser uses a gain jet, Rhodamine 6G dissolved in ethylene glycol, and a saturable absorber jet, DODC Iodide dissolved in ethylene glycol. An argon laser tuned at 514.5 nm is used to pump the gain jet and provide amplification. The saturable absorber provides a nonlinear medium whose absorption decreases with increasing light intensity. When a pulse of light travels through the absorber jet, the absorber is bleached and the absorption is temporarily modulated. The modulated absorption causes the transmitted pulse to be modulated. The pulse modulates the absorber and the absorber in turn modulates the pulse. [23] This modulation is automatically synchronized with the laser cavity round-trip time. The ring geometry provides another mode-locking mechanism by supporting two counter-propagating pulses. The laser has the highest efficiency when the clockwise and counter-clockwise pulses collide at the absorber jet. The absorber will saturate the most because the two pulses cause a standing-wave interference pattern to occur at the saturable absorber. The pulse will collide in the absorber when the dye jets for the gain medium and the saturable absorber are separated by one-quarter of the total cavity length [24]. This insures that the two pulses will not collide in the gain jet. Passing through the gain jet at different time will cause the pulses to receive the maximum amplification. The intracavity prisms are mounted on translation stages and are used to change the group-velocity

dispersion [22]. Translating the prism normal to its base changes the amount of intracavity quartz that the beam travels through and thus changes the group-velocity dispersion.

The CPM generates about 4-10 mW of power out of each arm of the ring cavity at a repetition rate of 100 MHz for a 99 % output coupler. A typical operating bandwidth spans from 606 nm to 626 nm with a peak at 619 nm and a FWHM of 10 nm. This bandwidth produces a pulse that has a FWHM of 97.5 femtoseconds.

3.2 Frequency Spectrum Measurements

Being able to measure the frequency spectrum of a femtosecond laser is very important. It can give information that can be used to determine if the laser is generating short pulses and can give a general idea of the width of the femtosecond pulse. Part of the output generated by CPM is monitored by a Optical Multi-channel Analyzer and the frequency spectrum is displayed on a computer screen. A optical fiber is placed outside of the CPM laser cavity and a beamsplitter is used to direct output light into the fiber. The fiber directs the light to a monochromator. The monochromator takes the input beam and spreads out the frequency components onto a linear photodiode array. The signal from the photodiode array is processed by a computer program. The resulting intensity versus photodiode location is plotted onto a computer screen. The individual photodiodes correspond to specific frequency components. A laser with a known wavelength(such as a HeNe) is directed into the fiber and the photodiode that detects the light corresponds to the specific wavelength of the laser. This is done with a few other photodiodes, and a calibration can be generated to convert location of the photodiode to wavelength. The computer program uses this calibration to then plot the intensity versus wavelength. This is very useful, because it displays the spectrum of the CPM. The spectrum of the laser gives much information about the output pulse. If the spectrum is very short, that means the laser is not producing short pulses and needs to be adjusted. The CPM laser is at optimum operation when it has a stable spectrum that is $\sim$ 20 nm wide and is centered at 620 nm.

3.3 Pulse Width Measurement

It is very important to be able to measure the pulsewidth generated by ultrashort pulse lasers. Many techniques have been developed using nonlinear crystals to obtain a pulse width measurement [25] [26] [27]. Two very important diagnostics that are used to characterize the pulsewidth is the real-time autocorrelator [28] and the cross correlator.

3.3.1 Autocorrelator

The autocorrelator continuously displays an autocorrelation function that can be used to monitor the output of the laser. The output of the CPM is also sent to an autocorrelator for the purpose of measuring the pulsewidth.

The autocorrelation geometry is shown in figure 3.2. The setup consists of a Michelson-like arrangement in which a beamsplitter is used to split the light into two arms that are delayed relative to each other and polarized orthogonally to each other [26]. The reference beam is sent to a fixed translation stage and retroreflected. The signal arm of the autocorrelator is directed to a pair of parallel "spinning mirrors" mounted on two ends of a disk rotating at a constant angular frequency. The reference pulse is also retroreflected and is reflected by the pair of mirrors to the beamsplitter. Rotation of the disk provides a time-dependent path length for the signal pulse. This provides a variable delay between the two pulses. At the beamsplitter, the signal and reference pulse meet so they are exactly parallel and co-propagating. The two parallel beams are focused by a lens onto a nonlinear crystal(KDP). The KDP crystal is oriented at such angle so that second harmonic generation(SHG) is produced when both polarizations intersect inside the crystal. The SHG signal is detected by a photomultiplier tube(PMT). The SHG signal is measured versus the variable time delay between the two arms on an oscilloscope. A signal is detected at the PMT when the variable delay between the two pulses is close to zero. The variable time delay causes the signal pulse to "sweep" across the reference pulse.

The signal at the PMT gives a direct measurement of the second order autocorrelation function of the intensity G^2 [29]. This second order autocorrelation is

$$G^2(\tau) = \frac{< I(t)I(t+\tau) >}{< I^2(t) >}.$$

The time delay between the two pulses is τ. As seen by the equation, $G^2(\tau)$ is symmetric for all possible I(t). So if the incoming pulseshape I(t) is known to symmetric, the actual shape could be deduced by $G^2(\tau)$.

For all of autocorrelations(and cross-correlations) done for these experiments, the pulseshape is assumed to have a $sech^2$ shape. The width given by the autocorrelator is a convolved pulsewidth. To compute the actual pulsewidth, the relation between the autocorrelation and the actual pulse must be determined. For the $sech^2$ pulsewidth, the second order autocorrelation function detects a signal that has a full width half maximum(FWHM) that is 1.55 times the FWHM of the actual pulse. Dividing the FWHM of the autocorrelation by 1.55 produces the deconvolved pulsewidth.

The autocorrelator needs to be calibrated to determine the exact relationship between the time scale on the oscilloscope and the actual time scale. In order to do this, the translation stage on the reference arm of the autocorrelator is varied. As the path length of the reference pulse is changed, the position of the autocorrelation pulse on the oscilloscope moves along the time axis. The path length divided by the speed of light gives the actual time change. The comparison of the two times will produce the conversion between the actual time and the oscilloscope time. For the autocorrelator used in the lab, the conversion is 1 μsec on the oscilloscope equals 4.32 fsec. So, the actual pulsewidth of the laser is the oscilloscope pulsewidth times 4.32 fsec/μm divided by 1.55. All the pulsewidths described in this paper will reflect this calibration and deconvolution.

The real time autocorrelator is an invaluable tool in the lab and enables one to adjust the CPM dye laser and see the effect that it has on the resulting pulsewidth. The autocorrelator and the spectrum displayed on the OMA provide feedback to see if the CPM is producing short pulses and the actual pulsewidth of those short pulses.

3.3.2 Cross-correlator

Autocorrelation are used to measure the pulsewidth generated by the laser, but the pulse width and shape of the pulses needed to be measured at various other times(like after passing through a pulse shaper). A cross-correlator is used to measure the pulse shape of a femtosecond pulse. It is very close in design to the autocorrelator with a couple of distinctions. The cross-correlation geometry is shown in figure 3.3. Two beams are also required for the cross correlation, but they are not the same beam as is with the case for the autocorrelator. One of the beams is the short pulse generated by the CPM, and is called the reference pulse. The other beam is the signal beam, which is the pulse that is to be measured. The signal beam is one that has been modified in some way and has some structure imposed on it. The signal and reference are again focused onto the nonlinear crystal and the second harmonic signal is measured. But for the cross-correlation, the variable delay is imposed onto the reference beam and used to "sweep" the reference pulse across the signal beam. This is done by a retroreflecting mirror attached to a motorized translation stage that is under computer control. The signal from the PMT is sent to a lock-in amplifier to detect very low signals and then input to the computer. The computer moves the retroreflector on the stepper motor and records the signal on the PMT as a function of the translation distance. After converting the translation length to a time delay, the signal from the lock-in amplifier is plotted versus time delay. The resulting display gives the output shape of the signal pulse and can be used to record the pulse shape that exits from a pulse shaper or any other medium that changes the pulse.

The reference pulse is usually the shorter of the two pulses. So, the reference pulse can be considered to be a delta function that is used to map out the signal pulse. Because the beams are not the same, the cross-correlation is not symmetric and can actually show pulse shape and pulse width unlike the autocorrelation which only shows pulse width. Since the cross-correlation has a translation stage that is computer controlled, the output is not displayed in real time. This is because the

computer has to record the signal, perform numerous calculations and then display the output onto the screen.

The entire experimental setup is shown in figure 3.4. One arm of the CPM is sent to the autocorrelator for diagnostic and the other arm is used for experiments. The second arm is split by a beamsplitter to provide a reference pulse for use in the cross-correlator. The beam that passes through the beamsplitter is sent to the pulse shaper. Then the output from the pulse shaper and the reference pulse is sent to the cross-correlator.

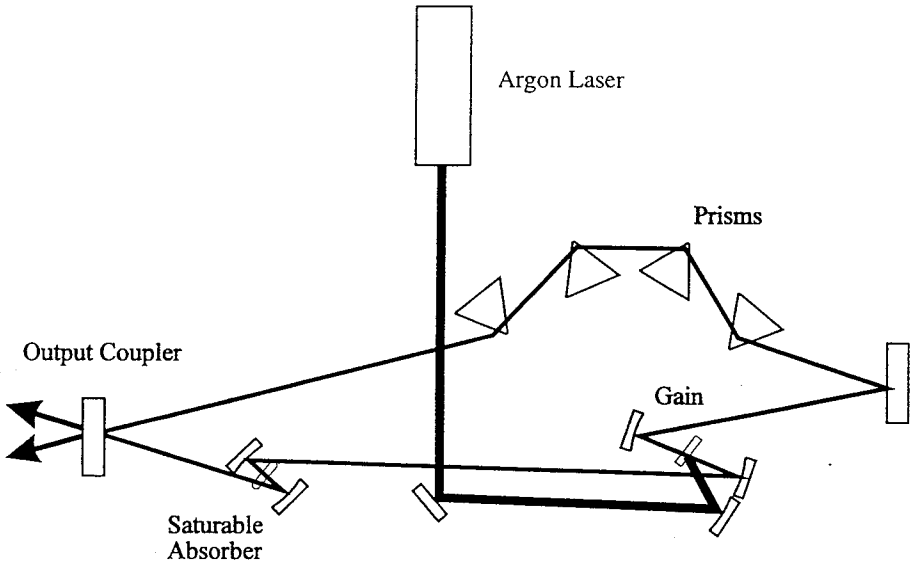

Figure 3.1 Colliding-pulse-mode-locked Dye Laser

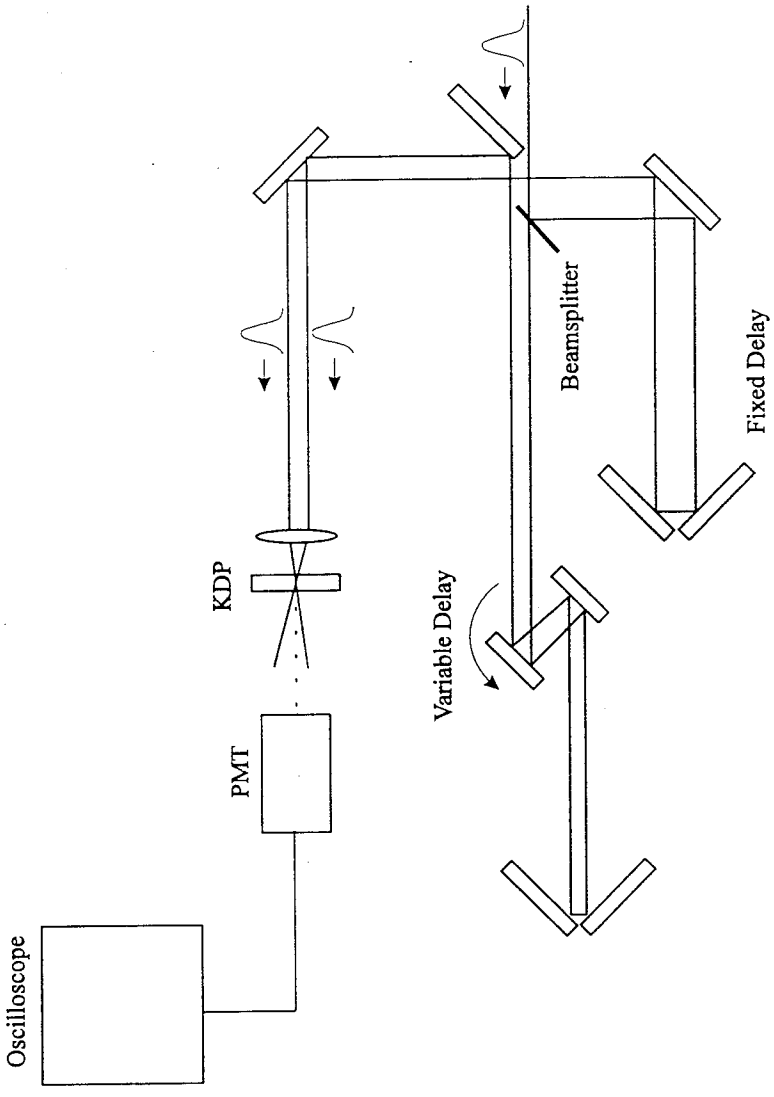

Figure 3.2 Real Time Autocorrelator

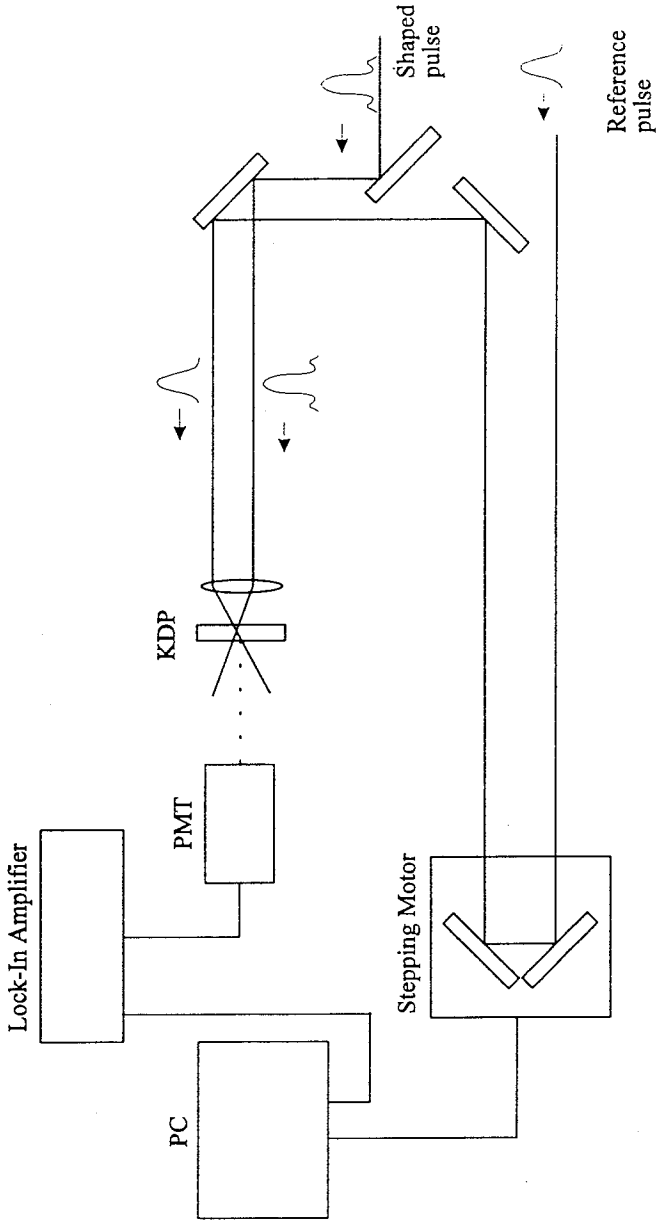

Figure 3.3 Cross-correlator

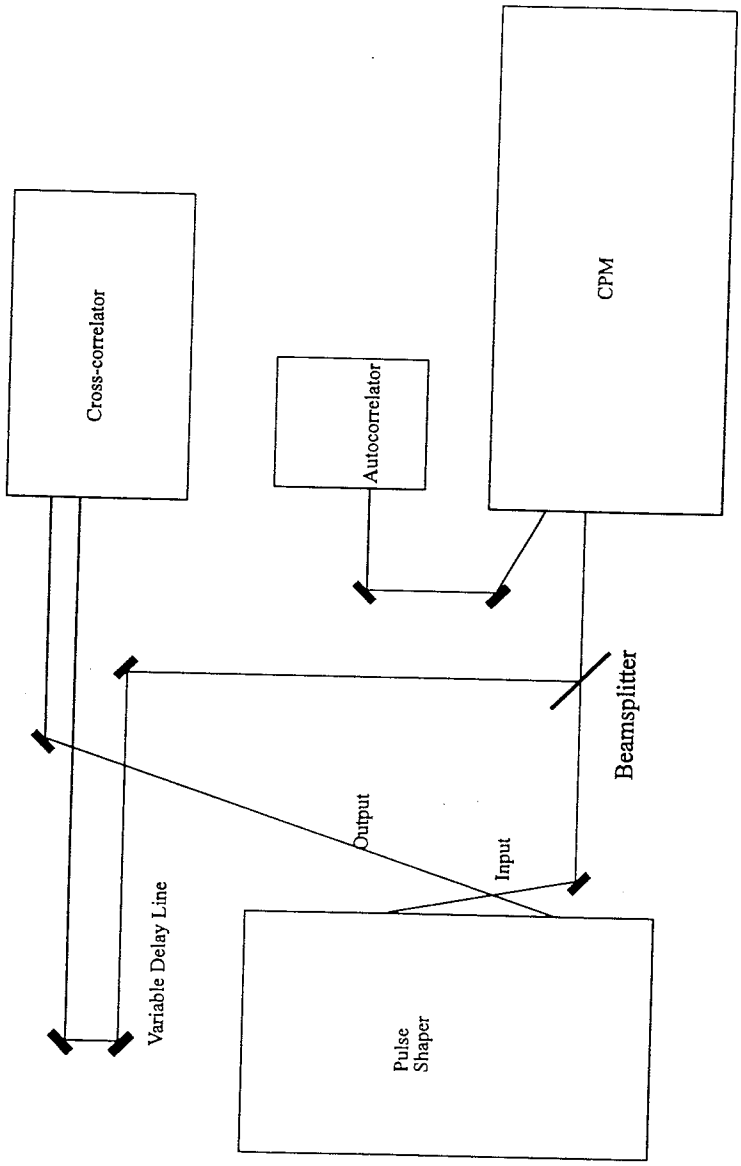

Figure 3.4 Experiment Block Diagram

4. MICROLENS ARRAYS

4.1 Fabrication Techniques

Microlithography has advanced to the degree that it is now possible to produce lenses with very small diameter. Miniature lenses have been fabricated that have diameters ranging from 2 mm to 99 μm. These have been produced as binary optics lenses [6] and as distributed index lenses [4]. Binary optics produces multiple diffraction orders that spread the power out over more than one direction. In my experiments, I concentrated on using distributed index lenses because of their inherent high coupling efficiencies.

One technique to make microlens produces arrays of small diameter spherical lenses, in a continuous material using a photothermal technique [5] [30] [31]. Detailed studies have been done to characterize the imaging performed by microlens fabricated by this method [10]. The lenses are formed by UV light which enables one to use photolithographic technology to produce an array that has a specific geometry. A sample of these microlens arrays was obtained from Corning Inc. but was unsuitable because the technique that exposes the material with UV light also causes the unexposed regions to be opaque. The opaque region would considerably reduce the efficiency of the microlens array if used within a pulse shaper. The microlens arrays also had a minimum separation 10-15 μm, which is too large for these experiments.

Microlens have also been produced on a planar glass substrate using an ion exchange technique [7]. A dopant is diffused into the substrate through a lithographic mask and forms a distributed-index in the radial and axial directions. With this method, many lenses or arrays of lenses can be produced on the substrate. These

microlens have been used with LCD projectors to improve efficiency [12]. These microlens arrays were obtained from NSG America and experimentally tested.

A third technique uses a relief master to mold optical epoxy microlenses on an optical substrate [4] [11]. A relief master is a lenslet pattern coined into an annealed and polished metal plate. The shape, radius of curvature, periodicity, and overall size of the mask can be designed to fit a specific application. The relief master is then used to mold an optical epoxy so that it conforms to the exact shape. This epoxy is affixed to an optical window or similar substrate. Microlens sizes range from 80 μm to 1 mm and focal lengths from 25μm to 260 mm. The microlens are configured in square and hexagonal arrays. These microlens arrays are produced by United Technologies.

4.2 Experimental Imaging Characteristics

To test the efficiency of the microlens array, a HeNe laser was used in the setup shown in figure 4.1. This preliminary experiment was used to analyze the various microlens arrays and determine which technique produced the microlens array with the highest efficiency. The HeNe was directed through one microlens array and retroreflected by a mirror. A beamsplitter was used to pick off the retroreflected beam so that it could be measured by a power meter at detector 1. The laser power was also measured at detector 2 to record any fluctuations caused by the light reflecting back into the laser cavity.

I have experimentally determined that microlens arrays fabricated using the optical epoxy give a better performance in terms of focusing and collimating a laser beam than the ones produced by ion exchange. An output spot could be produced using the microlens array formed from the optical epoxy, but could not be generated with the array formed by ion exchange. The output beam was similar to the Fraunhofer diffraction pattern for a square aperature [32]. The microlens formed by ion exchange are arranged in a hexagonal arrangement, which would not be beneficial when used with a one-dimensional modulator.

An on-axis and an off-axis case was analyzed. The reasoning behind this was that if the mirror and the microlens array were exactly perpendicular to the incoming laser beam, the retroreflected beam would go directly back into to the HeNe laser and change the effective reflectivity of the output coupler, which would change the output power of the laser. If the microlens and the mirror are tilted at a slight angle, the retroreflected beam will not go into the laser cavity.

The geometry was set for off-axis and the power was measured at detector 1 and 2. Without the microlens array in place, detector 2 measured the laser power at 2.7 mW and 1.5 mW was incident on detector 1. The microlens array was added and the distance between microlens and the back mirror was adjusted for maximum signal on the detector(separation equals microlens focal length). The output beam was a bright center spot with many dimmer spots arranged in the same geometry as the microlens array. The power measured at detector 2 was 3.0 mW and detector 1 measured .67 mW of power. The change in laser power, measured by detector 2, suggest that the dimmer spots around the bright center spot have provided feedback into the HeNe and changed the output power. In order to get a true measurement of efficiency of the microlens array, the fluctuations in power need to be addressed. The power reading at detector 1 can be normalized by the laser power(detector 2) to increase the accuracy of the output power measurement. The efficiency of the microlens arrays is defined as

$$\frac{\text{output power w/ microlens}}{\text{laser power w/ microlens}} \Big/ \frac{\text{output power w/o microlens}}{\text{laser power w/o microlens}}$$

or

$$\frac{\text{detector 1 w/ microlens}}{\text{detector 2 w/ microlens}} \Big/ \frac{\text{detector 1 w/o microlens}}{\text{detector 2 w/o microlens}}.$$

For the off-axis case, the microlens efficiency for two passes through the microlens array is 40.2%. This means that the efficiency through one microlens array is 63.4%. By using two detectors, the fluctuation in the laser power can be factored into the calculations and the feedback into the HeNe can be negated.

In the on-axis case, the retroreflected beam feeds back into the laser and increases the output power. Detector 2 measures 3.5 mW and output power is 1.65 mW when the microlens are not in place in the on-axis geometry. When the microlens are in place the laser power is 3.0 mW and the output power is .9 mW. The computed microlens efficiency for these values(using the above equation) for two passes through the arrays is 63.6%. Therefore the efficiency to go through one microlens array in the on-axis geometry is 79.7%.

The efficiency has been normalized, so the larger efficiency for the on-axis case can not be associated with the feedback. The normalization also takes care of the attenuation caused by reflectance and transmittance through the beamsplitter. The actual % reflected and % transmitted do not have to be measured for the beamsplitter, because they are factored into the efficiency by the normalization term. One possible cause of lower efficiency for the off-axis case is that the rays that enter a single microlens get retroreflected and pass back through the microlens at a different location or even a different microlens. This would cause the output beam to be composed of different rays than the input beam. By the above analysis, the microlens should be used in an on-axis geometry if possible to maximize efficiency. The reason why the efficiency is less than 100% can be explained by the description of the output beam. The numerous dimmer spots surrounding the central beam shows that the light is diffracted in many different directions. This causes the amount of light in the center spot to be a fraction of the total input power. In order to get higher efficiency, the dimmer spots surrounding the center spot must be eliminated or greatly reduced.

These microlens efficiency measurements are different than others that have been done. Some measurements have been done with raytracing [33] [9], optical fibers that match the center-to-center spacing of the microlenses [13], or in a geometry that is not possible for use inside a pulse shaper [8].

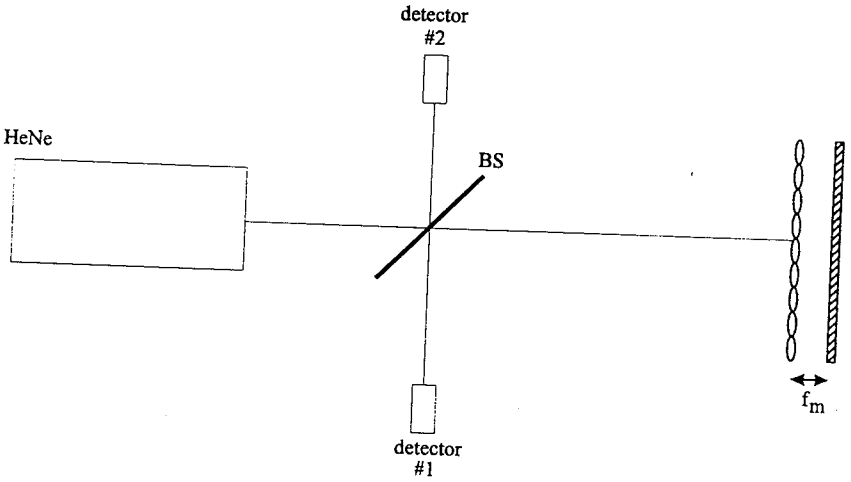

Figure 4.1 Microlens Array Testing using HeNe Laser

5. MICROLENS IN MODIFIED PULSE SHAPER

5.1 Introduction

Microlens could possibly be placed in a pulse shaper and used to maximize the efficiency of pixellated devices. Microlens arrays should be chosen that match the center-to-center spacing of the modulator pixels. These microlens can be used to direct the frequency components through the center of the modulator pixels and away from the interpixel dead space. Determining the correct geometry and spacing for the microlens is important to obtain the desired effect. Conventional ray-tracing can not be used because the pulse shaper contains dispersive elements (such as diffraction gratings) that cannot be modeled by ABCD matrices. A number of methods have been developed to model dispersive elements [34] [35] [16]. Using these methods the entire pulse shaping setup, from input grating to output grating, can be written as a product of matrices.

5.2 Ray-Pulse Matrices

5.2.1 Theory

A. G. Kostenbauder describes a way to expand the ABCD matrix to include terms for dispersive elements [16]. The conventional ray-tracing that describes the distance above the optical axis, x, and the angle a ray makes with the optical axis, θ, is modified to also include the frequencies, f, present in the pulse and the time it takes for a ray to travel a path length, t. Since the new ray-tracing still includes x and θ, the gaussian beam diameter can still be modeled as is done with the conventional ABCD matrices. The parameters at the output plane can be written as a function of

the parameters at the input plane. Using matrix algebra, it is written as

$$\begin{bmatrix} x \\ \theta \\ t \\ f \end{bmatrix}_{out} = \mathcal{F}\left\{ \begin{bmatrix} x \\ \theta \\ t \\ f \end{bmatrix}_{in} \right\}.$$

The matrix that performs the function on the input plane is written as the change in output parameter due to a change in the input parameter. It can be written as

$$\begin{bmatrix} x \\ \theta \\ t \\ f \end{bmatrix}_{out} = \begin{bmatrix} \frac{\partial x_{out}}{\partial x_{in}} & \frac{\partial x_{out}}{\partial \theta_{in}} & \frac{\partial x_{out}}{\partial t_{in}} & \frac{\partial x_{out}}{\partial f_{in}} \\ \frac{\partial \theta_{out}}{\partial x_{in}} & \frac{\partial \theta_{out}}{\partial \theta_{in}} & \frac{\partial \theta_{out}}{\partial t_{in}} & \frac{\partial \theta_{out}}{\partial f_{in}} \\ \frac{\partial t_{out}}{\partial x_{in}} & \frac{\partial t_{out}}{\partial \theta_{in}} & \frac{\partial t_{out}}{\partial t_{in}} & \frac{\partial t_{out}}{\partial f_{in}} \\ \frac{\partial f_{out}}{\partial x_{in}} & \frac{\partial f_{out}}{\partial \theta_{in}} & \frac{\partial f_{out}}{\partial t_{in}} & \frac{\partial f_{out}}{\partial f_{in}} \end{bmatrix} \begin{bmatrix} x \\ \theta \\ t \\ f \end{bmatrix}_{in}.$$

The 4 by 4 matrix can be simplified by evaluating the individual terms. The 4 terms in the upper left hand corner express the output displacement and angle in terms of the input displacement and angle. These are the conventional ABCD matrix elements.

For a time invariant system, $f_{out} = f_{in}$, which makes the bottom line 0, 0, 0, 1. Also, due to time invariance, the third column is 0, 0, 1, 0, because the displacement, angle, and frequency do not depend on the input time. This simplifies the expression to

$$\begin{bmatrix} x \\ \theta \\ t \\ f \end{bmatrix}_{out} = \begin{bmatrix} A & B & 0 & \frac{\partial x_{out}}{\partial f_{in}} \\ C & D & 0 & \frac{\partial \theta_{out}}{\partial f_{in}} \\ \frac{\partial t_{out}}{\partial x_{in}} & \frac{\partial t_{out}}{\partial \theta_{in}} & 1 & \frac{\partial t_{out}}{\partial f_{in}} \\ 0 & 0 & 0 & 1 \end{bmatrix} \begin{bmatrix} x \\ \theta \\ t \\ f \end{bmatrix}_{in}.$$

The remaining derivatives are named E through I to simplify the notation. These derivative can be analyzed for various optical components and a complete library of matrices can be used to analyze any optical system.

$$\begin{bmatrix} x \\ \theta \\ t \\ f \end{bmatrix}_{out} = \begin{bmatrix} A & B & 0 & E \\ C & D & 0 & F \\ G & H & 1 & I \\ 0 & 0 & 0 & 1 \end{bmatrix} \begin{bmatrix} x \\ \theta \\ t \\ f \end{bmatrix}_{in}$$

5.2.2 Common Matrices

Kostenbauder expands the conventional 2 by 2 matrix to 4 by 4 which allows one to define a matrix for gratings, prisms, and dispersive slabs as well as lens, mirrors, and free space. For completeness, the matrices for a lens, mirror and free space are listed. The 4 by 4 matrix for a lens or mirror is

$$\begin{bmatrix} 1 & 0 & 0 & 0 \\ -\frac{1}{f} & 1 & 0 & 0 \\ 0 & 0 & 1 & 0 \\ 0 & 0 & 0 & 1 \end{bmatrix}$$

and the matrix for free space is

$$\begin{bmatrix} 1 & d & 0 & 0 \\ 0 & 1 & 0 & 0 \\ 0 & 0 & 1 & 0 \\ 0 & 0 & 0 & 1 \end{bmatrix}.$$

where f is the focal length of the lens or mirror and d is the free space longitudinal distance along the optical axis. For non dispersive optics, the upper left corner is the conventional ABCD matrix and E through I are equal to zero. The above matrices do not give much more insight than the ABCD matrices.

When looking at grating and prism matrices, the value of the 4 by 4 matrices will become clearer. For a prism used at the tip with the ray exiting at normal incidence, the matrix is

$$\begin{bmatrix} m & 0 & 0 & 0 \\ 0 & \frac{l}{m} & 0 & -\frac{\partial n}{\partial f}\tan\psi \\ -\frac{\partial n}{\partial f}\frac{m\tan\psi}{\lambda_o} & 0 & 1 & 0 \\ 0 & 0 & 0 & 1 \end{bmatrix}.$$

where ψ is the prism apex angle, and $m = \cos\psi/\sqrt{1 - n^2\sin^2\psi}$.

The 4 by 4 grating matrix is

$$\begin{bmatrix} -\frac{\sin\phi}{\sin\psi} & 0 & 0 & 0 \\ 0 & -\frac{\sin\psi}{\sin\phi} & 0 & \frac{\cos\phi-\cos\psi}{f_o\sin\phi} \\ \frac{\cos\psi-\cos\phi}{c\sin\psi} & 0 & 1 & 0 \\ 0 & 0 & 0 & 1 \end{bmatrix}.$$

Figure 5.1 show the geometry that is used to define the input and output angles for the grating. The angle the incoming ray makes with the grating surface is ψ and ϕ is the angle from the outcoming ray to the grating surface, c is the speed of light in free space, and f_o is the center wavelength. Using the grating relationship $f_o(\cos\phi - \cos\psi) = \frac{c}{\lambda_{grating}}$ the grating matrix can also be written as

$$\begin{bmatrix} -\frac{\sin\phi}{\sin\psi} & 0 & 0 & 0 \\ 0 & -\frac{\sin\psi}{\sin\phi} & 0 & \frac{c}{\lambda_{grating}f_o^2\sin\phi} \\ -\frac{1}{\lambda_{grating}f_o\sin\psi} & 0 & 1 & 0 \\ 0 & 0 & 0 & 1 \end{bmatrix}.$$

By considering an input beam that is translated(different x) but has the same angle, frequency, and input time as a reference beam onto a grating, A, C, and G are computed. As the input angle is changed on a grating relative to a reference beam, B, D and H are calculated. If an input pulse has the same x and θ as the reference pulse but is detuned in frequency, the output time and position are the same which makes E = I = 0. A grating angularly separates frequencies, so it is known that F is nonzero. By looking at the ray geometry and differentiating the grating equation, F can be determined.

These matrices are the basic elements used to compute the matrix for any optical system. I have used the grating, free space, and lens matrices to compute the system matrix for a conventional pulse shaper. This was done to prove that the 4 by 4 matrices present an accurate analysis and can be used to compute a set of matrices that to be used to design the modified pulse shaper setup.

5.3 Analysis of Conventional Pulse Shaper

The conventional pulse shaper system is made up of seven matrices and can be written as

$$\begin{bmatrix} x \\ \theta \\ t \\ f \end{bmatrix}_{out} = G \cdot F \cdot L \cdot F \cdot F \cdot L \cdot F \cdot G \cdot \begin{bmatrix} x \\ \theta \\ t \\ f \end{bmatrix}_{in}$$

or

$$\begin{bmatrix} x \\ \theta \\ t \\ f \end{bmatrix}_{maskplane} = F \cdot L \cdot F \cdot G \cdot \begin{bmatrix} x \\ \theta \\ t \\ f \end{bmatrix}_{in}$$

$$\begin{bmatrix} x \\ \theta \\ t \\ f \end{bmatrix}_{out} = G \cdot F \cdot L \cdot F \cdot \begin{bmatrix} x \\ \theta \\ t \\ f \end{bmatrix}_{maskplane}$$

where the 4 by 4 matrices are denoted by G for grating matrix, F for free space, and L for lens. The angle the input and output beams make with the first grating are ψ_1, and ϕ_1. Similarly, ψ_2 and ϕ_2 are the angles the input and output beam make with the second grating. For the theoretical computations, ψ_2 is 60^o, $\phi_1 = \psi_2$, $\phi_2 = \psi_1$, $\lambda_{grating}$ is 1/(1800 lines/mm), L is 150 mm, f = 150 mm, and f_o is $\frac{c}{630nm}$. The system matrix for the pulse shaper should be dispersionless and generate a collimated output beam. The second form is useful because x, θ, t and f at the maskplane are calculated. These parameters can be used to analyze the effect of spatial filtering at the maskplane. The

computed system matrices for the maskplane and the output plane are

$$\begin{bmatrix} x \\ \theta \\ t \\ f \end{bmatrix}_{maskplane} = \begin{bmatrix} 0 & -d & 0 & \frac{cd}{\sin\psi_1 f_o^2 \lambda_{grating}} \\ 1/d & 0 & 0 & 0 \\ \frac{-1}{\sin\psi_1 f_o \lambda_{grating}} & 0 & 1 & 0 \\ 0 & 0 & 0 & 1 \end{bmatrix} \begin{bmatrix} x \\ \theta \\ t \\ f \end{bmatrix}_{in}$$

$$\begin{bmatrix} x \\ \theta \\ t \\ f \end{bmatrix}_{out} = \begin{bmatrix} -1 & 0 & 0 & 0 \\ 0 & -1 & 0 & 0 \\ 0 & 0 & 1 & 0 \\ 0 & 0 & 0 & 1 \end{bmatrix} \begin{bmatrix} x \\ \theta \\ t \\ f \end{bmatrix}_{in}$$

From the output system matrix, it is obvious that the pulse shaper adds no dispersion to the input pulse. The derivative I, $\frac{\partial t_{out}}{\partial f_{in}}$, is a measure of dispersion and is equal to zero which agrees with experimental and theoretical results of the pulse shaper. The ray-tracing analysis of the conventional pulse shaper is plotted in figure 5.2. Figure 5.2 is a plot of the transverse position of various frequencies versus position on the optical axis for a 3 mm input beam. The location of the maskplane is shown by the dashed line.

5.4 Analysis of Modified Pulse Shaper

When adding the microlens arrays in the pulse shaper, the unique characteristics of the pulse shaper must be preserved. Specifically, the zero-dispersion and collimation of the output beam cannot be altered. Zero-dispersion is important because even a small dispersion will cause the individual frequency components of the ultrashort pulse to travel at different speeds. The result of the frequency-dependent velocity is broadening of the femtosecond pulse. The beam must also be collimated to provide a stable beam width that will not change as it propagates. The frequency components must be recombined at the same spatial position they were at before the passed through the microlens array. In other words, the location of the frequency components

must be in the same order as they were previously. No frequency component may be swapped with another frequency component.

When using the 4 by 4 matrices for microlens array, a couple of techniques need to be applied. The matrices depend on the four parameters(x, θ, t, f) to compute the correct output. When dealing with the diffraction grating and the bulk lens, these parameters are defined in exactly the same way. The key parameter that will be different for the microlens array as compared to the bulk lens is x, the distance above the optical axis. There are many microlens spaced across the diameter of the bulk lens. When the 4 by 4 matrix is calculated for the microlens, x must be defined in terms of distance above the optical axis of the individual microlens. Therefore every x position in the global(grating, lens) ray-tracing matrix must be converted to a local(microlens) position. This is done after the rays travel through the free space distance after the bulk lens. The conversion must also be done after the last microlens array, to convert the local x back to the global value so that it can be used with the matrices for the second lens and grating. The other parameters (θ, t, and f) are exactly the same for the microlens array as for the bulk lens and grating.

To satisfy the zero-dispersion and beam collimation requirements, multiple computer simulations were run with various geometries. The rays in the pulse shaper were plotted as they travel through the optical components as a function of frequency and input beam width. By looking at the ray-tracing plots, the correct geometry could be decided and tested theoretically. The geometry that will exactly collimate the beams and insure zero-dispersion is one that is shown in figure 5.3. Four sets of microlens arrays are needed to perform the correct operation. The four microlens arrays are spaced apart from each other at twice the microlens focal length. The distance from the bulk lens to the first microlens array is the sum of their focal lengths. There is a plane of symmetry halfway between the middle two microlens arrays at the dotted line. This means that the distance from the fourth microlens array to the second bulk lens is also the sum of the two focal lengths. The first grating diffracts the light and spreads the frequency components of the femtosecond pulse into a fan shape. The

bulk lens collimates the frequency components in the plane perpendicular to the lines on the diffraction grating and focuses the frequency in the plane parallel to the lines on the diffraction grating.

Figure 5.4 shows a plot that includes the center part of the modified pulse shaper that includes the microlens arrays. The input beam diameter at the input grating was set at 3 mm. For this plot, the microlens diameter and center-to-center spacing is 100 μm, and the focal length of the microlenses is 1.7 mm. This is just an example of typical microlens parameter and is presented as an illustration of the correct geometry. Each cone of rays pictured in the figure is a different frequency component composed of rays that represents various input x (corresponding to a input beam with a finite width). The bulk lens focuses the rays that make up an individual frequency component to a series of discrete spots(In actuality, there is a continuous line of frequency spots, but to decrease computation time, the frequency components are discretized) The first microlens is placed one focal length from the bulk lens focus. This means that the distance from the bulk lens to the first microlens array is the sum of the lens focal length and the microlens array focal length. This causes the rays within that frequency to be collimated towards the center of the lens. The second microlens array takes the collimated beam and focuses it at the plane of symmetry. The rest of the pulse shaper is a mirror image of the first half. There is a plane of symmetry halfway between the second and third array at the dotted line. The third array collimates the rays towards the center of the microlens and the fourth array takes the collimated beam and focuses it at a plane that is exactly one lens focal length from the bulk lens. As shown by figure 4.2, the output rays on the right side appear the same as the input rays on the left. The 4 by 4 system matrix for the modified pulse shaper with the microlens arrays is

$$\begin{bmatrix} x \\ \theta \\ t \\ f \end{bmatrix}_{out} = \begin{bmatrix} -1 & 0 & 0 & 0 \\ 0 & -1 & 0 & 0 \\ 0 & 0 & 1 & 0 \\ 0 & 0 & 0 & 1 \end{bmatrix} \begin{bmatrix} x \\ \theta \\ t \\ f \end{bmatrix}_{in}$$

The individual matrix terms are expressed symbolically. The values used to do the computation are $\phi_1 = \psi_2$, $\phi_2 = \psi_1$, $\lambda_{grating}$ is 1/(1800 lines/mm), and f_o is $\frac{c}{630nm}$. In this calculation, the dispersion term, $\frac{\partial t_{out}}{\partial f_{in}}$, is again equal to zero. This proves that placing the microlens arrays in the described geometry does not add any dispersion to the pulse shaper.

The geometry described above produces a collimated output beam and preserve the zero-dispersion characteristics of the pulse shaper.

5.4.1 Location of Maskplane

The modified pulse shaper must be designed so that frequency components are directed so that they form a one-dimensional array of spots that correspond to the pixels of a modulating device. When looking at figure 5.4, keep in mind that the focused spots at the left and right side of the plot as well as the spots at the plane of symmetry are caused by the discretization of the continuous frequency spectrum. Actually, these three planes are a continuous line of spots. That fact must be kept in mind when looking at the arrangement and deciding where a pixellated device should be placed to maximize the effect of the microlens arrays. Between the first and second microlens array at the dashed line in figure 5.4, the rays are collimated and pass through the center region between the microlens arrays. This provides a location where the continuous line of frequency components is separated into an series of spots. Even when the rays that make up the frequency intersect the boundary between two microlens, the rays split and collimate in such a way that they avoid the spaces at the microlens boundaries and collimate toward the center of the microlens. Therefore, the continuous frequency spread should also be collimated away from the boundaries of the microlens and toward the center. A pixellated modulator array that has the same center-to-center spacing as the microlens arrays could be placed at the dashed line between the first and second microlens arrays. Therefore, halfway between the first and second microlens array is the maskplane for the modified pulse shaper. The regions at the edge of the microlens that the rays avoid corresponds to the interpixel

gaps present in the modulator. These figures represent the ideal case. This is the best that these microlens arrays can perform. Imperfect boundaries and diffraction may affect how the microlens arrays actually perform in the modified pulse shaper. Using the ray-tracing analysis, the width of the "effective" spot at the proposed maskplane in figure 5.4 for a microlens that has a focal length of 1.7 mm and a 3 mm input beam was calculated to be 56.7 μm. Figures 5.5 and 5.6 show two other plots that use microlens that have focal lengths of 1.1 mm and 1.0 mm and diameters of 99 μm and 200 μm. These microlens arrays were chosen because they have small diameters, comparatively large focal lengths, and provide a linear array that is longer than 5 mm. By looking at the two figures, it can be seen that the effective spot is smaller and smaller. The calculation for the spot size for figure 5.5 and 5.6 is 36.7 μm and 33.3 μm, respectively. So, as the focal length of the microlens decreases, the effective spot size also decreases. The limit on the spot size is determined by the values of focal lengths that can be produced for a microlens array.

Figures 5.4 through 5.6 are all commercially produced microlens arrays by United Technologies. The effective spot size and focal length are two parameters to consider when deciding on the best microlens array to use in the experiment. I decided to use the microlens array with 100 μm diameter and 1.7 mm focal length. This microlens array has the longest focal length and still provides a good spot size relative to the diameter of the microlens. The focal length is a major consideration because a spatial mask must be placed between the first and second microlens. Since this distance is twice the microlens focal length, the longer the focal length the more room to insert a spatial mask.

5.4.2 Gaussian Beam Analysis

The ABCD law for gaussian beam was used to give an indication of the gaussian beam diameter for a individual frequency component at various optical components [36]. A plane wave was assumed at the input grating and an expression was obtained for the beam waist at the first microlens array as a function of the beam

waist at the grating. The beam waist at the maskplane was also calculated as a function of the beam waist at the grating. The beam waists were doubled to get the beam diameter and shown as a table in figure 5.7. The input beam out of the CPM laser can be magnified or demagnified to produce the desired input beam diameter at the input grating. The location of the maskplane is like a telescope, so the beam diameter at the maskplane is f_m/f_l times the beam diameter at the grating.

The reason that this gaussian beam analysis is done is to calculate when an individual frequency component stays within the boundaries of one microlens. The frequency components need to be smaller than the microlens diameter in order to collimated and pass through one modulator pixel. If the beam diameter of a frequency component is larger than the microlens, the frequencies will be sent to many different modulator pixels and would not be able to be controlled by the modulator. By looking at the table, it is clear that the input beam diameter on the grating should be greater than 2.5 mm in order to be smaller than the microlens diameter (100 μm) at the microlens plane. The beam diameter at the microlens array plane is a minimum at 5.5 mm. The beam diameters at the maskplane are all smaller than the microlens diameter until the input beam diameter at the grating becomes ridiculously large. So, the size of the beam at the microlens array plane is the limiting case for this gaussian beam analysis. Ideally, the input beam should 5.5 mm to provide the smallest beam diameter at the microlens array plane and have a reasonable beam diameter at the maskplane. But, as long as the input beam diameter is 2.5 mm or greater, the beam diameter at the microlens array plane is sufficient.

5.5 Experimental Results

The experimental setup to test the modified pulse shaper is shown in figure 5.8. The modified pulse shaper is oriented in the reflection geometry instead of the transmission geometry shown in Figure 5.3. The output pulse travels in the opposite direction of the input pulse and is separated from the input with a beamsplitter. Since the modified pulse shaper has a plane of symmetry, placing a mirror at that

plane is exactly the same as duplicating the rest of the pulse shaper. The reflection geometry is used because it enables the use of two microlens arrays instead of four. This considerably reduces the number of optical elements that need to be aligned. When the microlens arrays are added to the pulse shaper, the alignment is very important. The most important is the lateral alignment of the microlens with respect to each other. This ensures that the two arrays exactly match one-to-one with each other. Slight misalignment will cause a decrease in the output signal strength because the mismatch of the microlens centers will not put the beams back together correctly. The spacing between the two microlens arrays is another important alignment. The microlens arrays must be spaced at exactly twice the microlens focal length. This is important to insure that the effective spot size is between the first and second microlens and that the beams will follow the paths shown in figure 5.4.

The diffraction grating has 1800 lines/mm, the bulk lens is an achromat that has a 150 mm focal length, and the microlens array has 100 μm diameter lens with a 1.7 mm focal length. Initially, the pulse shaper was aligned in the reflection geometry without any microlens array. The spacing between the grating and the bulk lens is adjusted to ensure zero dispersion, while the mirror-bulk lens spacing was set for a collimated output. The mirror was moved back four times the microlens focal length to make room for the pair of microlens arrays. The set of microlens arrays were placed inside the modified pulse shaper and coarsely adjusted to the correct spacing. A HeNe laser was aligned so that the beam was perpendicular and was used to pass through the two microlens arrays and coarsely align the vertical and horizontal alignment and focal distances between the two arrays. Femtosecond pulses from the CPM laser were then input to the modified pulse shaper. The vertical and horizontal position of the microlens arrays was adjusted to provide a collimated output beam.

Cross-correlation measurements were taken with and without the microlens arrays inside the pulse shaper. Figure 5.9 is a cross correlation of the output pulse width without the microlens. The deconvolved pulsewidth is 87 fsec (assuming $sech^2$). Figure 5.10 shows a cross-correlation that was recorded with the microlens array in

place. The deconvolved pulsewidth of 95 fsec shows that the measured pulse does not broaden considerably. The accuracy of the cross correlation is around 10 fsec which would explain the difference in the pulsewidth measurements for the modified and conventional pulse shaper. Figure 5.11 shows the output pulse generated by the microlens array on a larger time scale. There are large sidelobes that are at approximately $\pm$ 4 psec. This exactly corresponds to an inverse frequency spread across one microlens. The $\frac{\partial \lambda}{\partial x}$ as calculated before is 3.03 nm/mm. Using this value, the 100 μm microlens spacing corresponds to satellite pulses at $\pm$ 4.3 psec. This agreement between experiment and theory shows that the sidelobes are caused by the edge of the microlenses. Adjusting the horizontal and vertical positioning of the microlens arrays relative to each other minimizes the sidelobes. As seen by the bottom plot in figure 5.11, when the lenslets are misaligned the height of the sidelobes increases. At optimum alignment (the top plot in figure 5.11) the height of the sidelobe generated by the modified pulse shaper is 5.83 % of the center pulse maximum. This can be compared to the calculation shown in Figures 2.4 through 2.8. For a modulator that has 10 % dead space between the pixels, the sidelobe height at $\pm$ 4 psec is 1.19 % of the maximum. The values for 20 % and 30 % are 6.50 % and 16.70 %, respectively. For a modulator array that has 50 % deadspace the sidelobe height at $\pm$ 4 psec is 50.01 %. By comparing the heights of the sidelobes for the experimental results with the computer calculations for interpixel deadspace, we see that the microlens array has an "effective" diameter of about 85 μm caused by diffraction and aberrations caused by the edge of the individual microlenses. The "effective" diameter could be increased if the microlens were fabricated so that the edges of the individual microlenses conformed closer to a spherical surface.

The results of the HeNe testing of the microlens array will give rough measurement of how much power is expected to be output when the microlens arrays are used inside a pulse shaper. After double passing through one microlens array, the output efficiency is 63.6 %. The on-axis geometry is used because it provides the highest efficiency and smaller effective spot size. The pulse shaper is configured in the reflection

geometry and the light passes through the microlens array four times. The projected power transmitted for the modified pulse shaper should the efficiency squared or 39 % if the array was used in two dimensions like the HeNe testing. The efficiency is greater for the one-dimensional case inside the modified pulse shaper because the light will only encounter the microlens boundaries in one dimension instead of two. The beam through the pulse shaper is transmitted and reflected by a beamsplitter so the measured power will be lower than the actual power. Power Fluctuations of the CPM laser are normalized by also measuring the CPM power. With the microlens arrays inside the pulse shaper, the output beam was .085 mW and the CPM power was 5.75 mW. The output beam was .12 mW and the CPM laser power was 4.0 mW when the microlens were not used with the pulse shaper. Using the equation previously used for the testing the microlens arrays with the HeNe, the calculated efficiency for four passes through the arrays was 49.2 %. This is higher than the 39 % predicted by the HeNe two-dimensional case. So, for the one-dimensional geometry the efficiency for one pass through the microlens array has increased to 83.9 %.

The increased resolution of the output pulse(by reducing the sidelobe heights) that the microlens provide is important. The reduction (or elimination) of the sidelobe pulses insures that the output has only one shaped pulse. Satellite pulses that occur before and after the center shaped pulse can produce false signals at a detector used to receive the signal. For example, if the shaped pulse is used as a bit stream, the satellite pulse might trigger a 1 when it should be a 0. Therefore the suppression of these satellite pulses are very important.

These experiments used the microlens arrays shown in figure 5.4, they have a diameter of 100 μm and a focal length of 1.7 mm. This means that there is 3.4 mm between the two arrays in which a mask or modulator may be placed. This limits the type of modulator that can be used with this particular microlens arrays. The modulator and the microlens arrays must be picked such that the thickness of the modulator and the focal length of the microlenses match. One possibility is to mold the optical epoxy directly onto the modulator. This would require precise alignment

in order to get the desired results. Products have been made that have two microlens arrays on opposing sides of a substrate [33]. The alignment required to do this might be sufficient to perform the same operation on a pixellated modulator.

The ray-tracing shown in figure 5.4 does not take into account diffraction effects. As noted in section 4.2, the output beam from the microlens arrays displays a Fraunhofer diffraction pattern for a square aperture. Therefore, one can assume that diffraction plays a big part with the rays that impinge on the edge of the microlens arrays. The rays in figure 5.4 that pass through the edge of microlens will be diffracted off at an odd angle and will not pass through the system of microlens arrays. These rays will be lost and result in a lower efficiency than is predicted in the ray-tracing analysis. The rays that pass through the center of the microlens are not diffracted and should act like the rays in figure 5.4.

5.6 Future Experiments

The addition of the microlens arrays in a pulse shaper enables one to perform further experiments to measure how well the microlens improve the pulse shape produced by pixellated modulators. Fixed masks with intentional interpixel dead space can be fabricated to simulate such experiments. The fabricated mask would be placed at the maskplane of the modified pulse shaper. The interpixel gaps will produce the results shown in figure 2.4 to 2.8 if inserted into a conventional pulse shaper. The same mask would be inserted into the modified pulse shaper. Comparison of the two results can be used to analyze the effect of the microlens arrays. I have started to fabricate masks with different amounts of interpixel dead space and will use them to analyze the performance of the microlens arrays for various interpixel gaps. I think the use of the microlens array should provide some substantial improvement for the masks that have 20 % and 30 % deadspace and should provide marginal improvement for the masks that have 10 % and 50 % deadspace. This is because the 10 % case might have a smaller deadspace than the deadspace in the microlens array caused by the "effective" diameter of the microlenses. The 50 % deadspace will only have

marginal improvement because the microlens arrays won't be able to produce a small enough effective focal spot to pass through a 50 μm gap.

Pulse shaping is used to generate complex wave forms like pulse trains [37] and square pulses [17]. Figures 5.12 and 5.13 demonstrate what effect the interpixel gaps have on a complex wave form. Figure 5.12 is the calculated temporal intensity for a 1 psec square pulse that uses a modulator with no interpixel deadspace between the pixels. Figure 5.13 shows the calculated effect that a modulator with 30 % interpixel space will generate. A sin(x)/x modulation at the maskplane is multiplied by a modulator array that has 70gap. The output intensity is plotted in figure 5.13. Like in figures 2.4 through 2.8, the output wave form has satellite pulses that occur before and after the center square pulse. The satellite pulses have the same square shape as the center pulse but have a lower amplitude and occur at different output time.

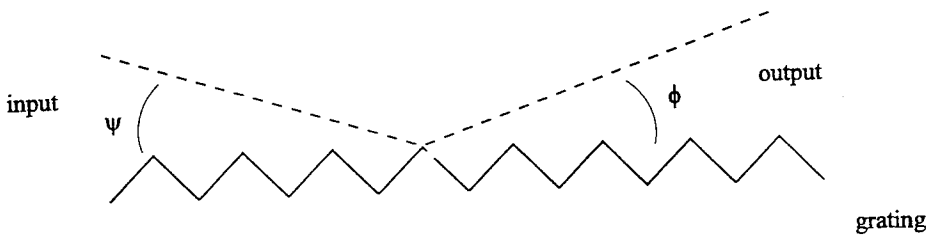

Figure 5.1 Grating Geometery for 4 by 4 Matrix

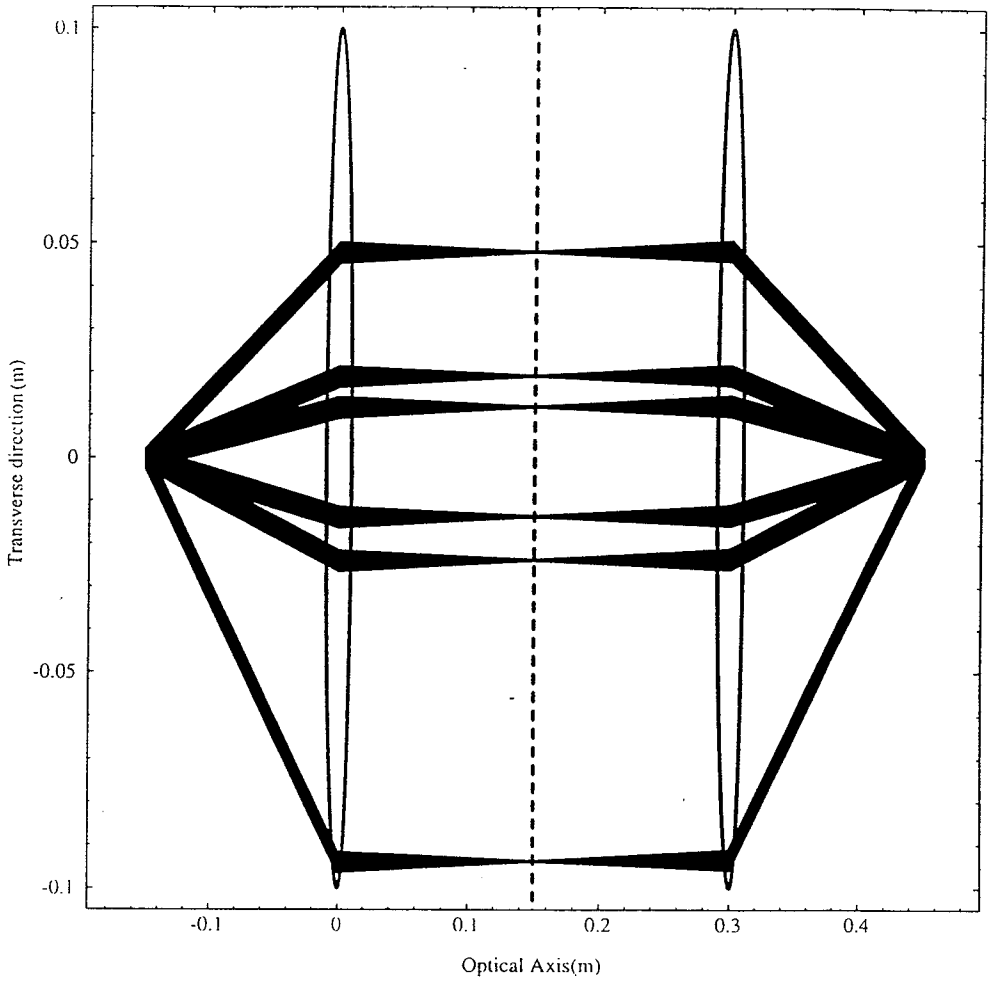

Figure 5.2 Ray Tracing of Conventional Pulse Shaper. The transverse direction is not typical and is only used for illustration

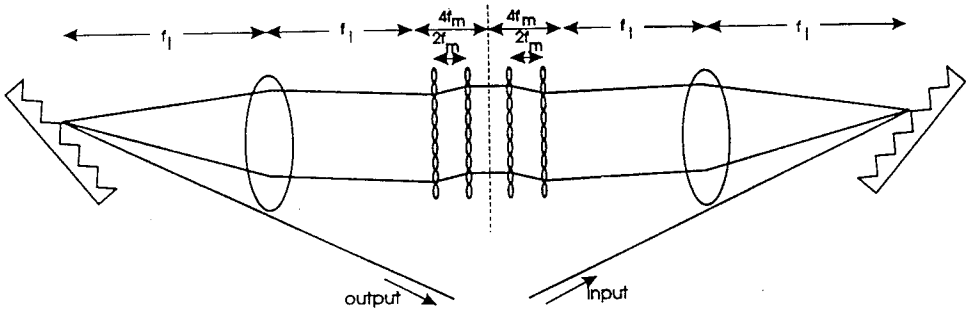

Figure 5.3 Modified Pulse Shaper Schematic

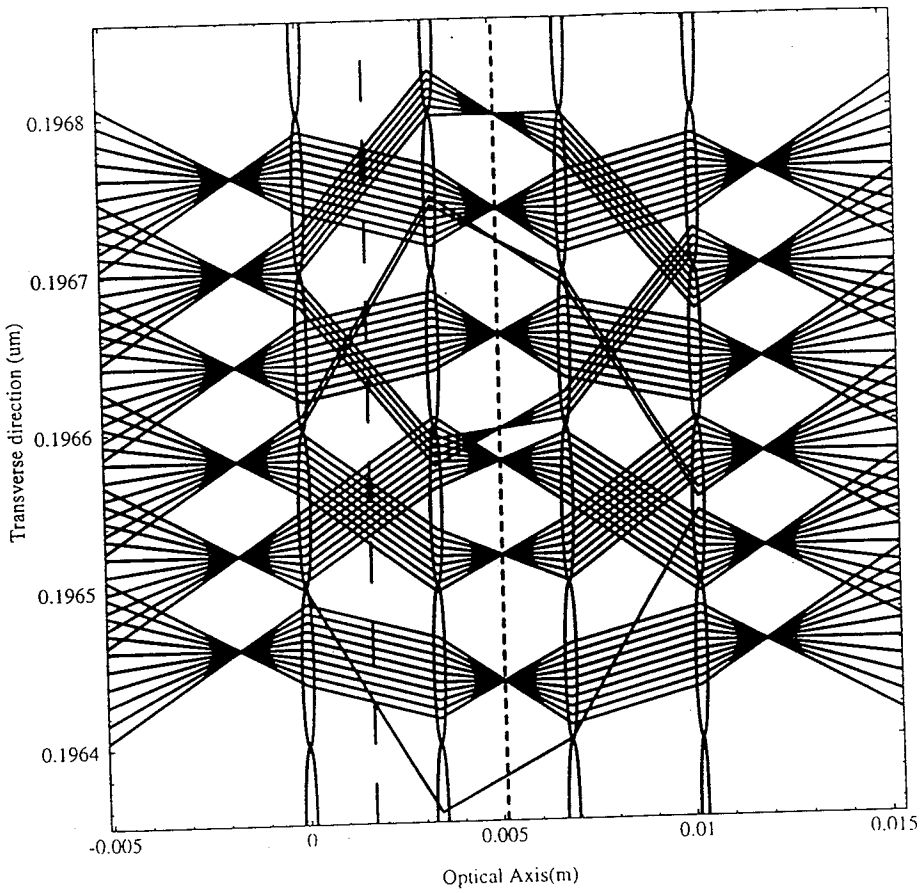

Figure 5.4 Ray-Tracing with 100 μm Diameter Microlens Array

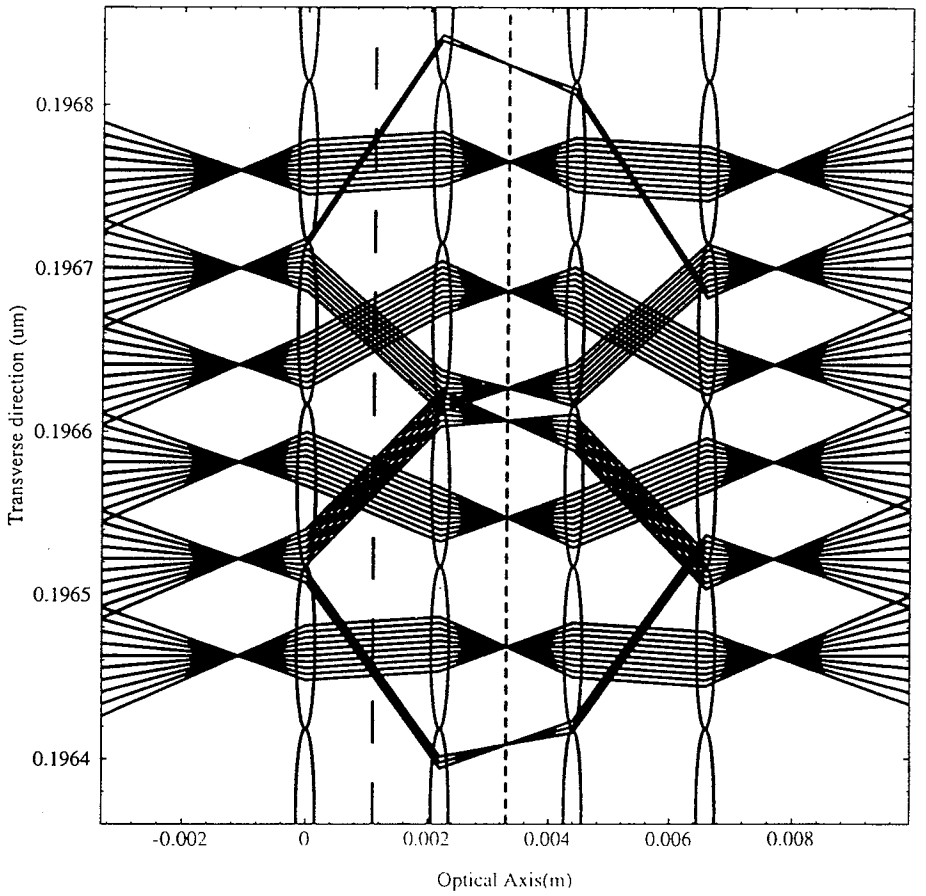

Figure 5.5 Ray-Tracing with 99 μm Diameter Microlens Array

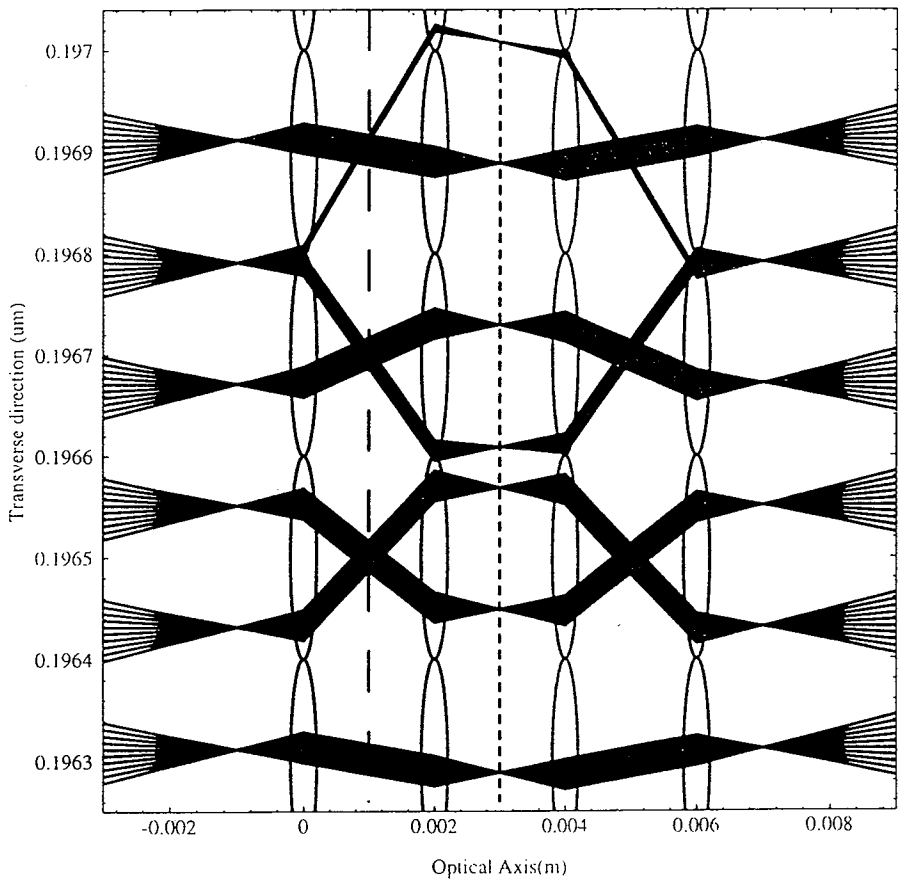

Figure 5.6 Ray-Tracing with 200 μm Diameter Microlens Array

Beam diameter at input (mm)	Beam diameter at microlens (μm)	Beam diameter at maskplane (μm)
.5	418.39	5.66
1.0	209.29	11.33
1.5	139.80	17.00
2.0	105.40	22.67
2.5	85.25	28.33
3.0	72.42	34.00
3.5	63.97	39.67
4.0	58.44	45.33
4.5	54.97	51.00
5.0	53.04	56.66
5.5	52.27	63.33
6.0	52.40	68.00

Figure 5.7 Table of Beam Diameter for Various Input Beams

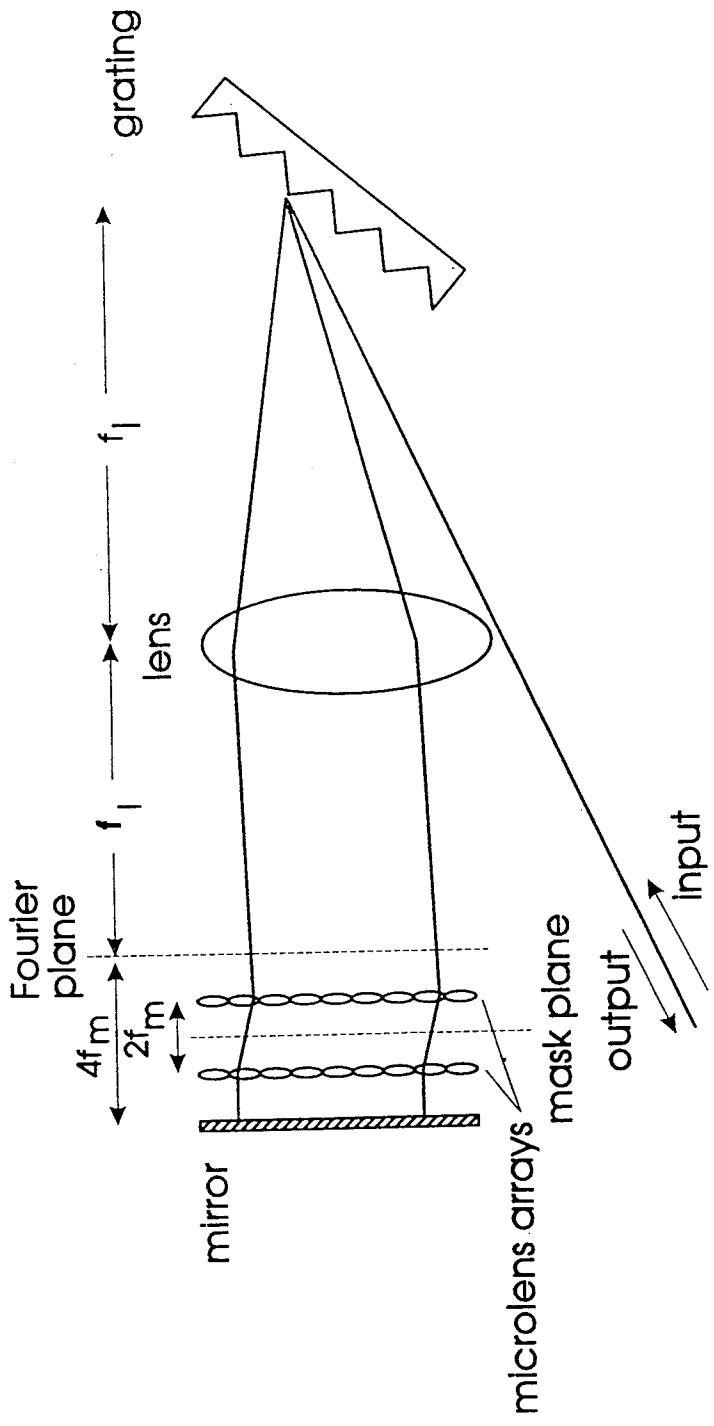

Figure 5.8 Modified Pulse Shaper in the Reflection Geometry

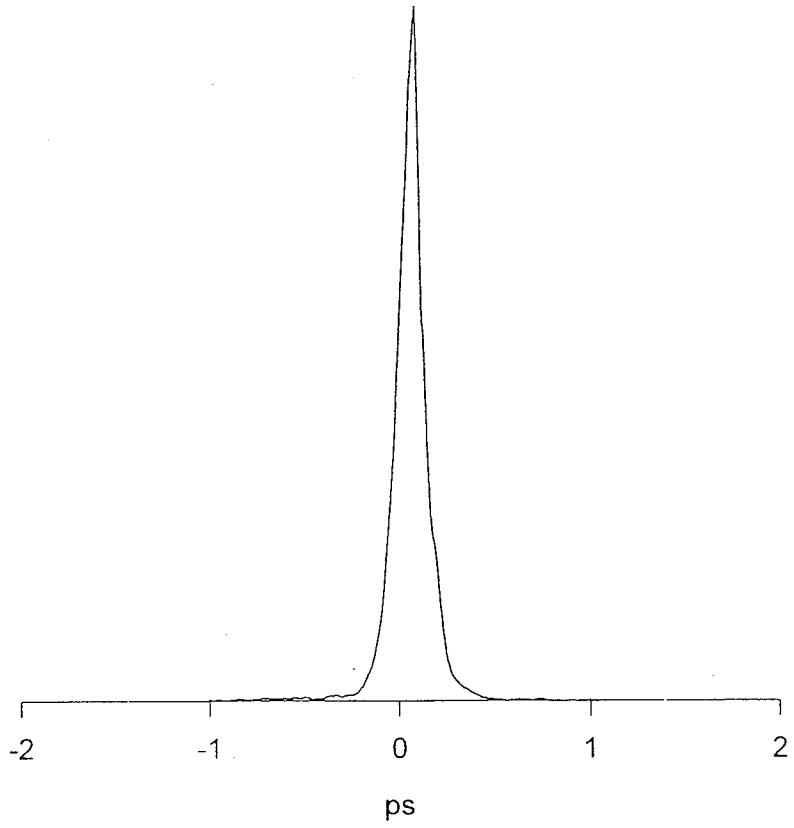

Figure 5.9 Cross-correlation of Conventional Pulse Shaper

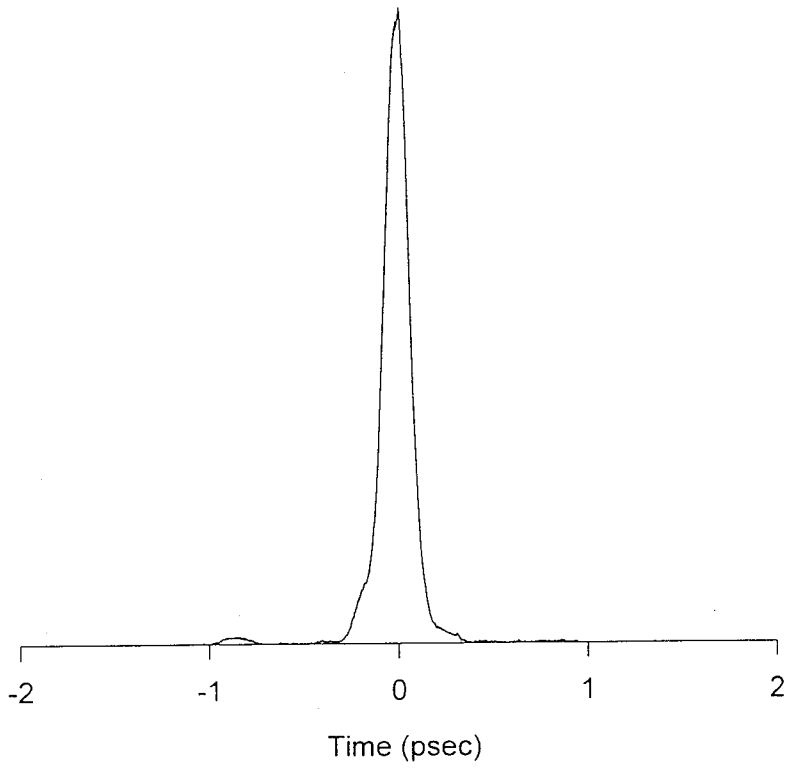

Figure 5.10 Cross-correlation of Modified Pulse Shaper

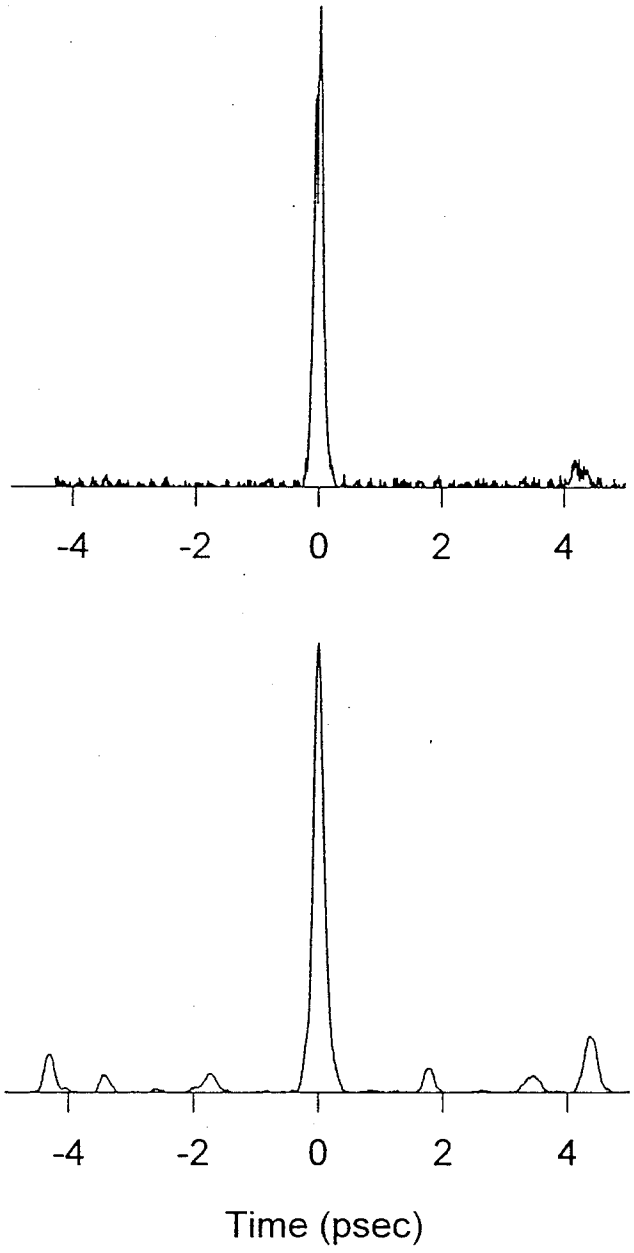

Figure 5.11 Sidelobes Generated by Modified Pulse Shaper

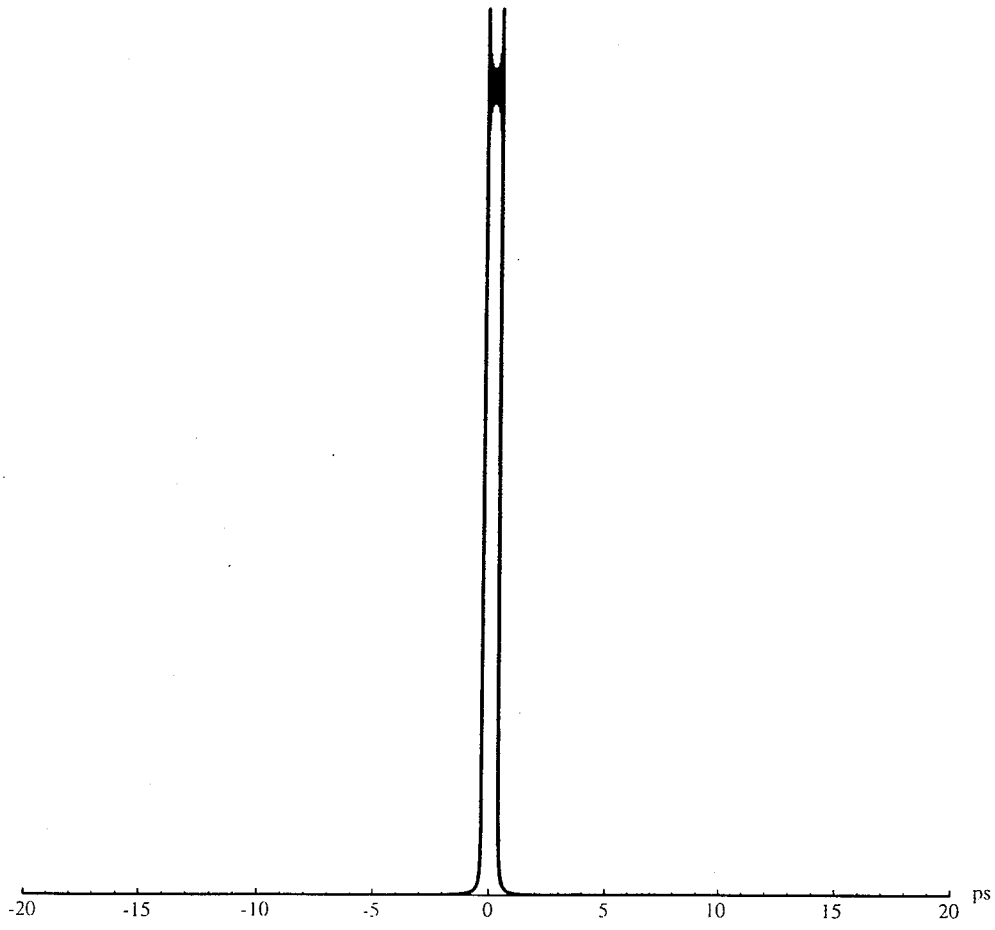

Figure 5.12 Complex Pulse Shape with 0 % Interpixel Space

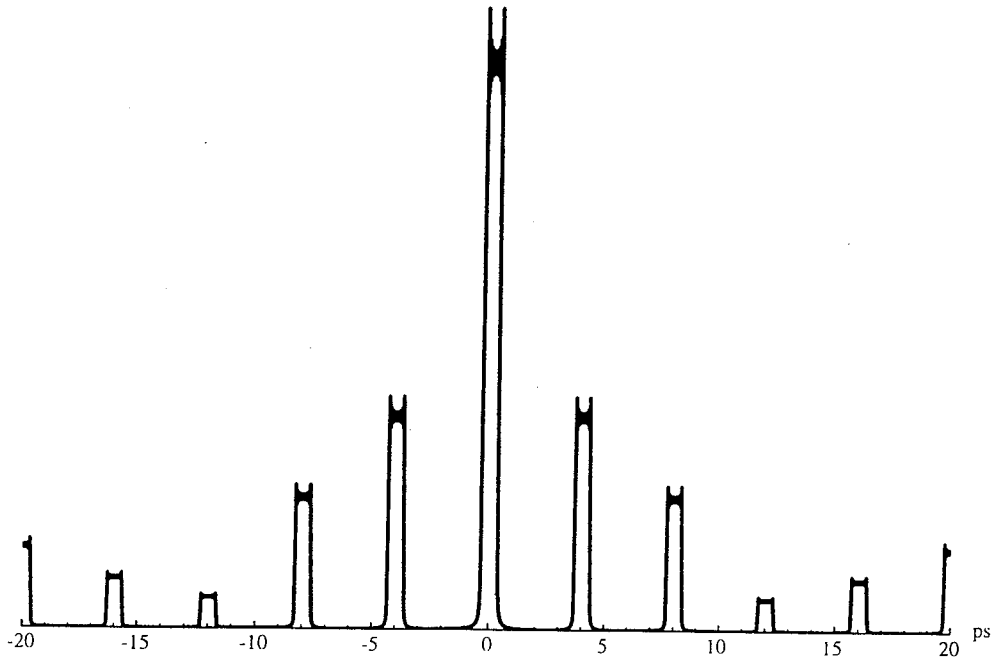

Figure 5.13 Complex Pulse Shape with 30 % Interpixel Space

6. CONCLUSION

A zero-dispersion grating compressor has been used as a femtosecond pulse shaper for many years. Fixed masks and modulator arrays have been used to spatially filter the frequency components that make up a ultrashort pulse. The use of modulator arrays, which have interpixel gaps, generates undesirable satellite pulses in a conventional pulse shaper. The height of the satellite pulses increases as the width of the interpixel gaps increases. Microlens arrays provide a possible solution to reduce the satellite pulses.

The microlens arrays can be made up of either binary optics lenses or distributed index lenses. The distributed index lenses are produced by photothermal techniques, ion exchange, or by molding an optical epoxy onto a substrate. The microlens arrays fabricated by the optical epoxy mold provide the highest efficiency and are best suited for addition into a pulse shaping setup. Experimental testing has shown that these microlens arrays have an efficiency of 40.2% when double passing through one microlens array in an off-axis geometry. When the setup is adjusted for on-axis geometry, the efficiency increases to 63.6%.

Ray-pulse matrices have been proven to be an accurate and convenient way to do ray tracing with dispersive elements. These matrices are used to generate computer calculations that model the modified pulse shaper and predict an optimum geometry. The specific geometry uses the microlens arrays to provide a effective focal spot for the modulator pixels and still preserves the non-dispersive properties of the pulse shaper. Four microlens arrays are needed if the pulse shaper is operated in the transmission geometry or two arrays are needed when operating in the reflection geometry. For the reflection geometry, the microlens arrays must be spaced at twice the microlens

focal length and the distance from the Fourier plane of the bulk lens to the back retroreflecting mirror must be four times the microlens focal length. The maskplane in the modified pulse shaper is between the two microlens arrays. This is where the spatial filtering should occur to produce shaped output pulses.

As shown experimentally, the use of microlens arrays does not introduce any dispersion onto the femtosecond pulse. Careful alignment of the microlens arrays is important to provide the best results. Slight misalignment causes satellite pulses to appear at the output. With the correct adjustments, these unwanted sidelobes can be greatly reduced. Experimentally, the height of the sidelobes is 5.83 % or less of the central pulse maximum. This is better than the value for the 80 μm pixels with 20 μm deadspace (6.50 %) but not as good as the 90 μm pixels with 10μm deadspace(1.19 %). The microlens seem to behave like a $\sim$ 85 μm diameter lens at 100 μm center-to-center spacing. The "effective" diameter could be increased if the diffraction effects at the edge of the individual microlens are controlled or reduced.

Future experiments using fixed masks that imitate pixels with various amounts of interpixel gaps should be provide more data that can be used to assess the performance of the microlens array. Since the modulator array needs to be placed between the two microlens array(which are spaced at twice the microlens focal length), the microlens focal length must be large enough to allow the thickness of a pixellated modulator to be positioned between the arrays. Because of the thickness of the modulator is a limitation, the possibility of molding the microlens directly onto the modulator array should be investigated.

LIST OF REFERENCES

LIST OF REFERENCES

[1] Andrew M. Weiner and J. P. Heritage. Picosecond and femtosecond fourier pulse shape synthesis. *Revue de Physique Appliqée*, 22(12):1619–1628, December 1987.

[2] Andrew M. Weiner, Daniel E. Leaird, J. S. Patel, and John R. Wullert II. Programmable femtosecond pulse shaping by use of a multielement liquid-crystal phase modulator. *Optics Letters*, 15(6):326–328, March 1990.

[3] Andrew M. Weiner, Daniel E. Leaird, J. S. Patel, and John R. Wullert II. Programmable shaping of femtosecond optical pulses by use of 128-element liquid crystal phase modulator. *IEEE Journal of Quantum Electronics*, 28(4):908–920, April 1992.

[4] Craig M. Schiller. *MLM Applications, Principles, and Design.* Adaptive Optics Associates, Inc., Cambridge, MA, 1992.

[5] Nicholas F. Borrelli, David L. Morse, Robert H. Bellman, and Walter L. Morgan. Photolytic technique for producing microlenses in photosensitive glass. *Applied Optics*, 24(16):2520–2525, August 1985.

[6] Kasra Rastani, Chinlon Lin, and Jay S. Patel. Active-fiber star coupler that uses arrays of microlenses and liquid-crystal modulators. *Applied Optics*, 31(16):3046–3051, June 1992.

[7] M. Oikawa. Distributed-index planar microlens array prepared from deep electromigration. *Electronics Letters*, 17(13):452–454, September 1981.

[8] D. Intani, T. Baba, and K Iga. Planar microlens relay optics utilizing lateral focusing. *Applied Optics*, 31(25):5255–5258, September 1992.

[9] Arnold J. Cantor, Mahmoud M. Abou el leil, and Robert H. Hobbs. Theory of 2-d ion exchange in glass: Optimization of microlens arrays. *Applied Optics*, 30(19):2704–2713, July 1991.

[10] N. F. Borrelli, R. H. Bellman, J. A. Durbin, and W. Lama. Imaging and radiometric properties of microlens arrays. *Applied Optics*, 30(25):3633–3642, September 1991.

[11] Dante D'Amato. Optical fabrication and testing. In *1990 Technical Digest Series, Volume 11.* Optical Society of America, June 1990.

[12] H. Hamada, F. Funada, M. Hijikigawa, and K. Awane. Brightness enhancement of an lcd projector by a planar microlens array. In *SID 92 Digest*, pages 269–272. Society for Information Display, 1992.

[13] J. S. Leggatt and M. C. Hutley. Microlens arrays for interconnection of single-mode fibre arrays. *Electronics Letters*, 27(3):238–240, January 1991.

[14] F. B. McCormick, F. A. Tooley, T. J. Cloonan, J. M. Sasian, H. S. Hinton, K. O. Mersereau, and A. Y. Feldblum. Optical interconnections using microlens arrays. *Optical and Quantum Electronics*, 24:S465–S477, 1992.

[15] Nörbert Streibl, Uwe Nölscher, Jürgen Jahns, and Susan Walker. Array generation with lenslet arrays. *Applied Optics*, 30(19):2739–2742, July 1991.

[16] A. G. Kostenbauder. Ray-pulse matrices: A rational treatment for dispersive optical systems. *IEEE Journal of Quantum Electronics*, 26(6):1148–1157, June 1990.

[17] Andrew M. Weiner, J. P. Heritage, and E. M. Kirschner. High-resolution femtosecond pulse shaping. *Journal of the Optical Society of America B*, 5(8):1563–1572, August 1988.

[18] C. W. Hillegas, J. X. Tull, D. Goswami, D. Strickland, and W. S. Warren. Femtosecond laser pulse shaping by use of microsecond radio-frequency pulses. *Optics Letters*, 19(10):737–739, May 1994.

[19] Andrew M. Weiner. Femtosecond spectral holography. *IEEE Journal of Quantum Electronics*, 28(10):2251–2261, October 1992.

[20] Andrew M. Weiner and Daniel E. Leaird. Generation of terahertz-rate trains of femtosecond pulses by phase-only filtering. *Optics Letters*, 15(1):51–53, January 1990.

[21] R. L. Fork, B. I. Greene, and C. V. Shank. Generation of pulses shorter than 0.1 ps by colliding pulse modelocking. *Applied Physics Letters*, 38(9):671–672, May 1981.

[22] J. A. Valdmanis, R. L. Fork, and J. P. Gordon. Generation of optical pulses as short as 27 femtoseconds directly from a laser balancing self-phase modulation, group-velocity dispersion, saturable absorption, and saturable gain. *Optics Letters*, 10(3):131–133, March 1985.

[23] A. M. Weiner and P. W. Smith. Mode-locking of lasers. In *Encyclopedia of Physical Science and Technology*, pages 456–469. Academic Press, 1987.

[24] Anthony E. Siegman. *Lasers.* University Science Books, Mill Valley, CA, 1986.

[25] J. A. Armstrong. Measurement of picosecond laser pulse widths. *Applied Physics Letters*, 10(1):16–18, January 1967.

[26] H. P. Weber. Method for pulse width measurement of ultrashort light pulses generated by phase-locked lasers using nonlinear optics. *Journal of Applied Physics*, 38(5):2231–2234, April 1966.

[27] A. Brun, P. Georges, G. le Saux, and F. Salin. Single-shot characterization of ultrashort light pulses. *Applied Physics*, 24(8):1225–1233, August 1991.

[28] Zafer A. Yasa and Nabil M. Amer. A rapid-scanning autocorrelation scheme for continuous monitoring of picosecond laser pulses. *Optics Communications*, 36(5):406–408, March 1981.

[29] S. L. Shapiro. *Ultrashort Light Pulses.* Springer-Verlag, Berlin, 1984.

[30] N. F. Borrelli and D. L. Morse. Microlens arrays produced by a photolytic technique. *Applied Optics*, 27(3):476–479, February 1988.

[31] R. H. Bellman, N. F. Borrelli, J. A. Dafin, G. Mann, and B. H. Raeder. Precision glass microlens array by a photo-thermal technique. In *Optoelectronics and Laser Applications in Science and Engineering.* SPIE O-E LASE, January 1988.

[32] Eugene Hecht. *Optics.* Addison-Wesley, Reading, MA, 1987.

[33] Dante D'Amato and Robert Centamore. Two applications for microlens arrays: detector fill factor improvement and laser diode collimation. In Chandrasekhar Roychoudhuri and Wilfrid B. Veldkamp, editors, *Miniature and Micro-Optics: Fabrication and Systems Applications*, pages 166–177. SPIE — The International Society for Optical Engineering, July 1991.

[34] Oscar Eduardo Martínez. Matrix formalism for pulse compressors. *IEEE Journal of Quantum Electronics*, 24(12):2530–2536, December 1988.

[35] Sol P. Dijaili, Andrew Dienes, and John Stephen Smith. Abcd matrices for dispersive pulse propagation. *IEEE Journal of Quantum Electronics*, 26(6):1158–1164, June 1990.

[36] Joseph T. Verdeyen. *Laser Electronics.* Prentice Hall, Englewood Cliffs, NJ, 1989.

[37] Andrew M. Weiner and Daniel E. Leaird. Generation of terahertz-rate trains of femtosecond pulses by phase-only filtering. *Optics Letters*, 15(1):51–53, January 1990.